Final Report
PI: Matthew Campen, Ph.D.
Affiliation: College of Pharmacy, University of New Mexico
Address: MCS09 5360, 1 University of New Mexico, Albuquerque, NM 87131
Award Institute: Health Sciences Center, University of New Mexico
Final Report completion: 23 November 2015
Grant Number: 1R21OH010495-01
Title: Endothelial Cells as Biosensors for Occupational Cardiovascular Risk

TABLE OF CONTENTS

LIST OF ABBREVIATIONS

ACh: Acetylcholine
ATP: Adenosine Triphosphate
BAL: Bronchoalveolar lavage
BBB: Blood Brain Barrier
CD36: Cluster of Differentiation 36
CNS: Central Nervous System
DM: Dispersion Media
eNOS: Endothelial Nitric Oxide Synthase
EPR: Electron Paramagnetic Resonance
FBS: Fetal Bovine Serum
ICAM-1: Intercellular Adhesion Molecule
iNOS: inducible Nitric Oxide Synthase
KPSS: Potassium Physiological Saline Solution
LDH: lactate dehydrogenase
LPS: Lipopolysacchride
MMP: Matrix Metalloproteinase
MWCNT: Multi-walled carbon nanotubes
mCECs: Mouse Cerebrovascular Endothelial Cells
MGD: N-methyl-D-glutamindithiocarbamate
NO: Nitric Oxide
PBS: Phosphate Buffered Saline
PM: Particulate Matter
VCAM -1: Vascular Adhesion Molecule

ABSTRACT

Engineered nanomaterials (ENMs) have an unknown toxic potential and the relationship between their biological effects and physicochemical properties remains uncertain. ENM inhalation studies have identified several potential systemic outcomes that are relevant to human health, including the development or exacerbation of inflammatory vascular disease / atherosclerosis, vasoconstriction, and neuropathies, possibly related to abnormal signaling in endothelial cells. However, ENMs translocate only minimally beyond the lungs, thus cardiovascular and neurological effects thereof may be caused by generation of secondary biomolecular factors from MWCNT-pulmonary interactions that spill over into the systemic circulation. The present study was implemented to develop a novel, translational *in vitro* model to assess systemic inflammatory changes caused by inhaled ENMs. Initial efforts focused on the optimization and development of assays based on cultured endothelial cells or isolated vascular tissue responses to whole serum, which represents a cumulative balance of anti- and pro-inflammatory factors. In two principal studies, we elucidated the utility of this general paradigm in terms of establishing a serum-borne inflammatory potential arising from pulmonary exposure to MWCNT and also in terms of establishing an improved mechanistic understanding of systemic outcomes. In the first application of this paradigm, wildtype (WT; C57BL/6) and MMP-9$^{-/-}$ mice were exposed to varying doses (10 or 40 μg) of MWCNTs (MWCNT-7) via oropharyngeal aspiration and serum was collected at 4 and 24 h post-exposure. Primary cerebrovascular endothelial cells treated with serum from MWCNT-7-exposed WT mice exhibited significantly reduced nitric oxide (NO) generation, as measured by electron paramagnetic resonance, an effect that was independent of NO scavenging. Serum from MWCNT-7-exposed WT mice inhibited acetylcholine-mediated relaxation of aortic rings at both time points, an effect dependent on vascular CD36 scavenger receptors. Interestingly, serum from MMP-9$^{-/-}$ mice exposed to MWCNT did not diminish the magnitude of vasorelaxation in naïve WT aortic rings. In the second application of this endothelial cell biosensor paradigm, WT and MMP-9$^{-/-}$ mice were again exposed to MWCNT-7 via pharyngeal aspiration, leading to enhanced hippocampal and cerebellar GFAP staining, indicative of astrocyte activation. MWCNT exposure impaired blood brain barrier integrity, as noted by fluorescein uptake, which was associated with increased gene expression of IL-6 and CCL5 in the cortex and hippocampus. Pretreatment with the rho kinase inhibitor, fasudil, was able to prevent brain fluorescein uptake and neuroinflammation. In vitro, serum from MWCNT exposed mice was able to induce expression of adhesion molecules at both the gene and protein level. Treatment of endothelial cells with serum from MWCNT-exposed mice in a wound-healing assay resulted in decreased cell motility and cytokinesis, also consistent with mRNA expression patterns in microarray analysis. Combined, these studies highlight the value of the endothelial cell biosensor paradigm as a valuable tool for dissecting the pathways connecting pulmonary exposures to ENMs and systemic vascular and neural effects. Future studies should further explore the mechanistic pathways and additionally utilize this assay platform for the confirmation of outcomes in occupationally exposed humans. Linkage of this assay platform to an information-rich discovery platform would be valuable for the determination of exposure-linked biomarkers.

EXECUTIVE SUMMARY

This project began with two independent objectives designed to establish a novel endothelial biosensor assay:

In Aim 1, we proposed to rigorously *optimize* an *in vitro* testing platform using three primary murine endothelial cell lines, focusing on expression of adhesion molecules and generation of NO. This involved selection of a maximally-responsive cell line (derived from aorta, coronaries, or cerebral vessels) and characterization of responses to known inflammatory stimuli. We also proposed to treat cells with serum from a known model of systemic inflammation to assess the range of responses.

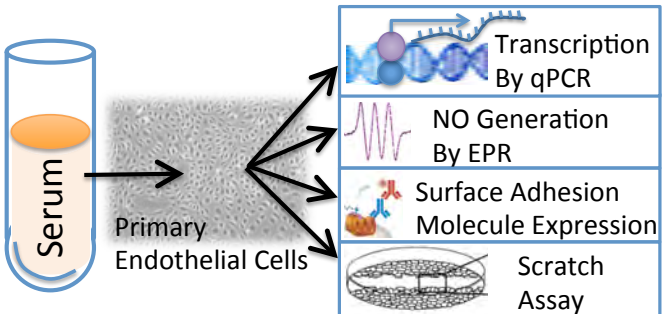

Figure 1. General assay paradigm for using endothelial cells as biosensors. Serum, in a dilute fashion, is incubated with confluent primary endothelial cells and a variety of responses, including transcriptional, functional, and translational, can then be assessed.

In Aim 2, we proposed to assess endothelial cell responses to serum obtained following pulmonary exposures of MWCNT and graphene. Exposures were largely executed by out collaborator at NIOSH (Erdely) and serum was shipped to our laboratory for this Aim. All responses in endothelial cells were related back to pathology and gene responses from the joint UNM/NIOSH work.

Aim 1 was focused on both optimizing and expanding the biosensor assay paradigm. For several reasons, we chose primary murine cerebrovascular endothelial cells after several parallel assays were conducted. The rationale for this choice involved factors related to the growth rate of the cells and the sensitivity to known cytokine mediators, in terms of specific canonical inflammatory transcripts. The other cell types (aortic, coronary endothelial cells) may well be of value in other applications, but the cerebrovascular endothelial cells were optimal for our studies. Over the course of the development, however, we expanded the assays beyond just transcriptional outcomes to examine functional outcomes, such as nitric oxide (NO) generation, expression of inflammatory surface markers by flow cytometry, and regrowth via a wound-healing or "scratch" assay (Figure 1).

For Aim 2, we conducted a few exploratory assays with graphene, as proposed, but results were less robust than those for MWCNT. Because the emphasis of this exploratory research grant was on establishing the value of this biosensor assay paradigm within a larger framework of mechanistic toxicological research, we allocated remaining resources to apply the assays developed in Aim 1 to integrate within a whole animal study. Two separate objectives were broached in this manner, 1) to examine serum bioactivity in terms of vasorelaxation and 2) to assess serum inflammatory potential on vascular endothelial cells as it pertains to cerebrovascular function.

In the first application of this biosensor paradigm, wildtype (WT; C57BL/6) and MMP-9$^{-/-}$ mice were exposed to varying doses (10 or 40 µg) of MWCNTs (MWCNT-7) via oropharyngeal aspiration and serum was collected at 4 and 24 h post-exposure. Primary

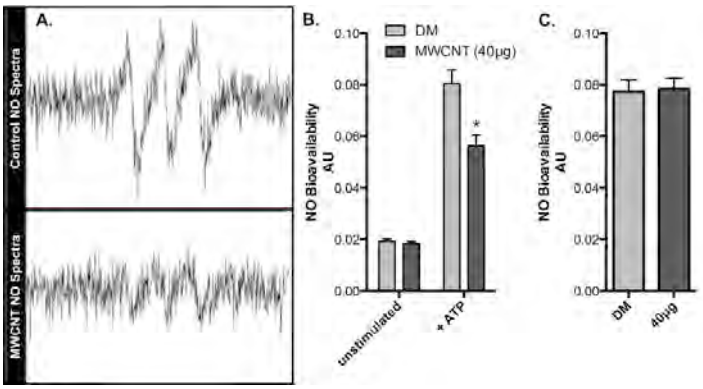

Figure 2. Effects of serum from MWCNT-7-exposed mice on NO generation and bioavailabilty. **A.** Representative EPR spectra from endothelial cells incubated with control serum and serum from MWCNT-7-exposed mice. **B.** Unstimulated endothelial cells exhibited minimal baseline levels of detectable NO, which was not different when incubated with serum from DM (control) or MWCNT-7-treated mice. However, when stimulated by ATP, endothelial cells incubated with control serum demonstrated a significantly greater capacity to generate NO than cells treated with serum from MWCNT-7-exposed mice (*$p<0.05$, N=3 per group). **C.** In an acellular assay, levels of NO in iron-free media containing a known concentration of the NO donor, spermine NONOate, were not different in the presence of serum from control or MWCNT-7-treated mice.

cerebrovascular endothelial cells treated with serum from MWCNT-7-exposed WT mice exhibited significantly reduced nitric oxide (NO) generation, as measured by electron paramagnetic resonance, an effect that was independent of NO scavenging (Figure 2). Additionally, we applied serum to naïve aortic rings mounted on force transducers (Danish MyoTechnology) to assess the relationship of this reduced NO generation to a functional outcome of vasorelaxation. Serum from MWCNT-7-exposed WT mice at both time points inhibited acetylcholine-mediated relaxation of aortic rings. This effect was dependent on vascular CD36 scavenger receptors, as naïve aortic rings from CD36$^{-/-}$ mice exhibited a complete relaxation curve regardless of whether serum from control or MWCNT-7-exposed mice was applied. Interestingly, serum from MMP-9$^{-/-}$ mice exposed to MWCNT did not diminish the magnitude of vasorelaxation in naïve WT aortic rings. We conclude that much of the observed bioactivity in serum arises from MWCNT-induced MMP-9 activation and the resultant degradation products. Ongoing proteomic research will attempt to address this in greater detail.

In the second application of this endothelial cell biosensor paradigm, WT and MMP-9$^{-/-}$ mice were again exposed to MWCNT-7 via pharyngeal aspiration, leading to enhanced hippocampal and cerebellar GFAP staining, indicative of astrocyte activation, in WT but not MMP-9$^{-/-}$ mice. MWCNT exposure also impaired blood brain barrier integrity, as noted by fluorescein uptake into the brain, which was associated with increased gene expression of IL-6 and CCL5 in the cortex and hippocampus. Pretreatment with the rho kinase inhibitor, fasudil, was able to prevent brain fluorescein uptake and neuroinflammation. *In vitro*, serum from MWCNT-exposed mice was able to induce expression of inflammatory adhesion molecules at both the gene and protein level (Figure 3). Genomics on the endothelial cells from these studies revealed a profile of upregulated genes consistent with inflammation and defense pathways, while downregulated genes were consistent with cell division and motility. Treatment of endothelial cells with serum from MWCNT-exposed mice in a wound-healing assay resulted in decreased cell motility and cytokinesis, also consistent with mRNA expression patterns in microarray analysis.

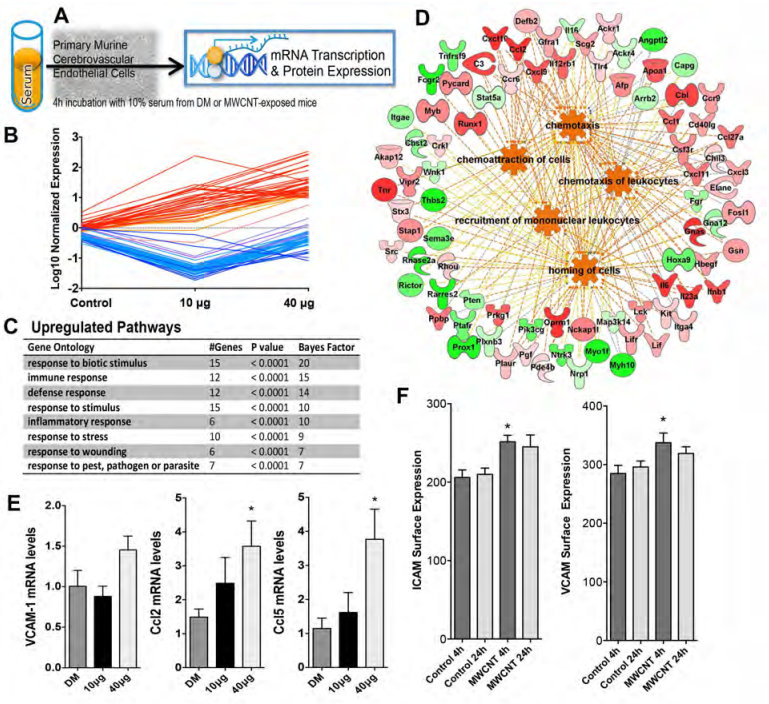

Figure 3. Inflammatory responses of cerebrovascular endothelial cells treated with serum from MWCNT-exposed mice. A. General depiction of assay protocol, with serum from exposed mice incubated on primary murine cerebrovascular endothelial cells. B. Microarray results indicate numerous transcripts (60) from serum-treated endothelial cells were elevated in a dose-dependent manner; elevated transcripts were ontologically related inflammatory and/or cellular defense response. C. Specific inflammatory genes responses from microarray results. D. Collective pathway integration from microarray. E. Confirmation of key inflammatory mRNA responses by PCR finds that endothelial VCAM-1, Ccl-2, and Ccl-5 mRNA were all significantly up regulated by serum from MWCNT-treated mice. F. Endothelial cell surface ICAM-1 and VCAM-1 protein expression were both elevated by serum from mice exposed to the 40µg dose of MWCNT as compared to control. Asterisks denote significant difference from DM control serum (P<0.05).

Combined, these studies highlight the value of the endothelial cell biosensor paradigm as a valuable tool for dissecting the pathways connecting pulmonary exposures to ENMs and systemic vascular and neural effects. Future studies should further explore the mechanistic pathways and additionally utilize this assay platform for the confirmation of outcomes in occupationally exposed humans. Linkage of this assay platform to an information-rich discovery platform would be valuable for the determination of exposure-linked biomarkers.

COMMUNICATIONS ARISING

Overall, the studies will be published primarily in two manuscripts and several abstracts/posters:

MANUSCRIPTS

1. Aragon MJ, Erdely A, Bishop L, Salmen R, Weaver J, Liu J, Hall P, Tracy Eye T, Kodali V, Zeidler-Erdely P, Stafflinger JE, Ottens AK, Campen MJ. MMP-9-dependent serum-borne bioactivity caused by multi-walled carbon nanotube exposure induces vascular dysfunction via the cd36 scavenger receptor. *Toxicol Sci*, in revision, 2015.
2. Aragon MJ, Topper L, Sanchez, B, Zychowski K, Herbert G, Hall P, Erdely A, Tracy Eye T, Zeidler-Erdely P, Stafflinger JE, Campen MJ, Ottens AK. Serum-Borne Bioactivity Caused by Inhaled Multiwalled Carbon Nanotube Exposure Induces Neuroinflammation Via Increased Blood Brain Barrier Permeability. In preparation.

ABSTRACTS

1. Campen MJ, Chen LC. Role Of Circulating Factors In Mediating Systemic Toxicity Of Inhaled Substances. Society of Toxicology, Phoenix, AZ, March 2014.
2. Aragon M, Erdely A, Campen MJ. Endothelial Cells as Biosensors to Assess the Systemic Inflammatory Impact of Multi Walled Carbon Nanotubes. Society of Toxicology, Phoenix, AZ, March 2014.
3. Campen MJ, Aragon M, Erdely A. Induction of Serum Inflammatory Potential by Pulmonary Exposure to Multi-Walled Carbon Nanotubes. American Thoracic Society, San Diego, May, 2014
4. Aragon M, Roberts JR, Erdely A, Campen MJ. Endothelial Cells as Biosensors to Assess the Vascular Inflammatory Potential of Serum Following Nanomaterial Exposure. Society of Toxicology, San Diego, CA, March 2015.

Additional manuscripts may also be forthcoming, as certain data, including graphene-related effects and alternative assays with other cell lines were not fully captured in these two communications.

ENDOTHELIAL CELLS AS BIOSENSORS FOR OCCUPATIONAL CARDIOVASCULAR RISK

1.1 INTRODUCTION

Pulmonary exposure to nanomaterials such as carbon nanotubes is associated with the progression of cardiovascular disease (Li et al. 2007). However, gaps exist in our understanding of the pathways by which inhaled substances affect the systemic vasculature, and this hinders our ability to predict risk and identify potentially vulnerable subpopulations. Inhaled nanomaterials, such as multi-walled carbon nanotubes (MWCNTs), have limited ability to translocate into the systemic circulation (Mercer et al. 2013) and evidence for a direct interaction between nanomaterials and vascular cells at relevant exposure concentrations is lacking. Several studies have demonstrated more profound systemic vascular effects arising from particle inhalation (Nurkiewicz et al. 2008; Nurkiewicz et al. 2009; Sun et al. 2005) as compared to gavage or even direct intravenous injection (Bai et al. 2007; Folkmann et al. 2012), suggesting that secondary, circulating factors induced by pulmonary responses to exposure contribute to adverse cardiovascular effects.

Central to the development of cardiovascular disease is the activation of the endothelium, characterized by the increased expression of adhesion molecules, extravasation of leukocytes, and the loss of endothelial nitric oxide synthase (eNOS) function (Aird 2008). eNOS produces the diffusible molecule nitric oxide (NO), which is anti-inflammatory, anti-coagulatory, and vasodilatory (Alheid et al. 1987; Kubes et al. 1991; Nunokawa and Tanaka 1992). In an atherosclerotic state, eNOS becomes “uncoupled” leading to the loss of NO bioavailability (Harrison 1994). Loss of NO enhances the pro-inflammatory environment that is central to the progression of atherosclerosis. Mounting evidence suggests that pattern recognition (e.g. TLR4) or scavenger receptors (e.g. CD36) play a prominent role in mediating endothelial activation (Shaul 2003; Wang et al. 2011). Lipid peroxidation products present in the lung lining fluid following exposure to particulate matter (PM) mediate systemic cellular inflammatory responses through Toll-like receptor 4, and such modified lipids have been shown to be present following exposure to concentrated ambient particulate matter (Kampfrath et al. 2011). CD36, a class B scavenger receptor, recognizes many ligands and is widely expressed on the surface of multiple cell types, including macrophages and endothelial cells (Febbraio et al. 1999; Sawada et al. 2012). CD36 is involved in atherosclerosis and inflammation (Febbraio et al. 2001) and is required for the endothelial dysfunction induced by inhalation to the reactive gas ozone (Robertson et al. 2013).

Additionally, inflammation in the cerebrovascular vessels has been shown to increase permeability of the blood brain barrier (BBB)(Takeda et al. 2014), a specialized structure composed of astrocytes, pericytes and endothelial cells that acts as a barrier between the brain and the rest of the body. Under normal conditions, the BBB prevents passage of undesired molecules from the bloodstream into the central nervous system (CNS). However, under inflammatory conditions(Calderon-Garciduenas et al. 2004), the tight junctions between the endothelial cells can become destabilized resulting in a leaky BBB and allowing peripheral inflammatory molecules to invade the CNS and activate the brain’s resident immune cells, specifically microglia(Bussy et al. 2015b) and astrocytes. Presently there are few studies investigating the link between inhaled toxicants and neuroinflammation. Oppenheim and colleagues found that inhalation of mixed vehicle emissions was able to induce BBB permeability, as well as increase levels of inducible Nitric Oxide Synthase (iNOS) and IL-1β in the parenchyma (Lund et al. 2009). Additionally, ozone exposure in rats

has been associated with lipid peroxidation in the hippocampus (Rivas-Arancibia et al. 2010). To our knowledge, no studies currently exist exploring the role of engineered nanomaterials in induction of neuroinflammation or BBB permeability.

One potential source of circulating ligands that interact with pattern recognition receptors following inhalation exposure is activation of matrix metalloproteinases (MMPs) in the lung and the generation of degradation byproducts (Su et al. 2000). MMPs have been shown to be involved in a wide range of biological processes including development, wound healing, and host defense (Dagouassat et al. 2012). MMP-9, an MMP that binds collagen based substrates, has been shown to be upregulated and activated following exposure to PM and PM-containing combustion mixtures (Lund et al. 2009; Lund et al. 2011; Su et al. 2000). Erdely and colleagues reported increased gene expression of MMP-9 in the lung, as well as an increase in circulating MMP-9 as a result of pulmonary MWCNT-7 exposure (Erdely et al. 2009). The pathophysiological relevance of MMP9 activation following pulmonary exposure to nanomaterials remains unknown.

Currently, no studies exist investigating the potential links between vascular dysfunction, neuroinflammation, MMPs, CD36, and nanomaterial exposure. We hypothesized that MWCNT-7 exposure activates MMPs in the lung, leading to the generation of circulating ligands that may directly impact vascular function through the CD36 receptor. To test this hypothesis, we applied an innovative ex vivo methodology for assessing potential cumulative effects of circulating mediators on vascular function. In this study, we demonstrated that MWCNT-7 exposure induces the generation of circulating bioactive factors that diminish stimulated NO production, impair vasorelaxation, and are not linearly associated with MWCNT-7 dose. We further hypothesized that, following MWCNT exposure, neuroinflammation arises due to increased BBB permeability caused by circulating factors. In this study, we demonstrated that MWCNT exposure induces the generation of circulating bioactive factors, leading to activation of the cerebrovasculature and inflammatory cells, as well as increased BBB permeability.

2. MATERIALS AND METHODS

2.1 Animals

Specific pathogen-free, male C57BL/6J and MMP-9$^{-/-}$ (B6.FVB(Cg)-Mmp9tm1Tvu/J) mice from Jackson Laboratory (Bar Harbor, ME) and CD36$^{-/-}$ mice (from Maria Febbraio, Cleveland Clinic, bred in-house) on a C57BL/6 background, bred in-house, were used in this study. C57BL/6J and MMP9$^{-/-}$ mice for exposures were housed in the AAALAC-approved NIOSH Animal Facility, while naïve mice (C57BL/6J and CD36$^{-/-}$) donating aortas were housed in AAALAC-approved facilities at the University of New Mexico. All mice were provided food and tap water ad libitum in ventilated cages in a controlled humidity and temperature environment with a 12 hr light/dark cycle. Animal care and use procedures were conducted in accordance with the "PHS Policy on Humane Care and Use of Laboratory Animals" and the "Guide for the Care and Use of Laboratory Animals" (NIH publication 86-23, 1996). These procedures were approved by the respective Institutional Animal Care and Use Committees of the National Institute for Occupational Safety and Health and the University of New Mexico.

Mice, 8 weeks of age, were treated via oropharyngeal aspiration with MWCNT (MWNCT-7 / Mitsui-7) at 0 µg, 10 µg, or 40 µg (n=12 for each group was needed to generate enough serum for all tests). The MWCNT were prepared in a physiologic dosing media (DM) for the vehicle that consisted of mouse serum albumin (0.6 mg/ml) and 1,2-dipalmitoyl-sn-glycero-3-phosphocholine (10 µg/ml) in PBS. The MWCNT used in this study, MWCNT-7, have been extensively characterized previously (Porter et al. 2010). Mice were euthanized at 4 and 24 h following pulmonary exposure. Serum was collected and the left lung lobe was ligated and removed to preserve for MMP-9 protein determinations. Bronchoalveolar lavage was performed on the right lung lobes and the first lavage supernatant was assessed for lactate dehydrogenase activity, albumin concentration, and MMP9 levels.

2.2 Fractionation and Mass Spectrometry

Serum was first processed through a 0.1 µm Ultrafree-MC filtration unit (EMDMillipore, Billerica, MA) per manufacturer instructions. The clarified serum (100 µL) was then processed through a pre-cleaned Amicon Ultra-0.5 centrifugal filter with Ultracel-30 membrane (EMDMillipore) per manufacturer instructions at 10°C. Filtered sera (n = 5 per 0, 10, 40 µg MWCNT-7 groups) were prepared for liquid chromatography - tandem mass spectrometry (LC/MSMS). Samples (32 µL) were acidified with 8 µL of 1% formic acid, with 4 µL loaded onto a Symmetry C18 reversed-phase trap column using a NanoAcquity UPLC (Waters, Milford, MA). Separation was performed with a 150 mm x 75 µm HSS T3 reversed-phase capillary column at 55°C online with a nano-electrospray equipped Synapt G2 HDMS tandem mass spectrometer (Waters). Separation and data-independent mass spectrometric analysis with ion mobility was performed as described previously (Fuller et al. 2012; Ottens et al. 2014) with the modifications that gradient elution was performed from 2% to 42% acetonitrile in water (formic-acid modified) and spectra were collected between 200 and 1800 m/z, with a collision energy ramp from 32 to 52 eV. All spectra were post-processed employing PLGS ion processing software (Waters). Generated ion tables were clustered and aligned by retention time (+/- 1.0 min), drift time (+/- 4 bins) and ion mass (MH+, +/- 12 ppm) using Isoquant software (v1.6 beta)

(Distler et al. 2014; Kuharev et al. 2014). Results were filtered to include only reproducible ion events (observed in four or more biological replicates per group). Ion mass tables per group were then evaluated and compared using histogram analysis with a minimum size of 500 Da.

2.3 Cell Culture

Mouse cerebrovascular endothelial cells (mCECs) were obtained from a commercial vendor (Cell Biologics) and maintained according to manufacturer's recommendations at 37° and 5% CO2 – 95 O2 with complete endothelial cell medium supplemented with 10% Fetal Bovine Serum (FBS). All experiments were performed between passages 3-8. Assays were batched by exposure to enhance consistency and comparability across samples.

2.4 Spin trapping of MCEC-generated NO using electron paramagnetic resonance.

To test the generation of NO, serum from control or MWCNT-7-treated mice (4h post) was added to the mCECs at a ratio of 1:9 (10%) with basal endothelial cell medium. Electron paramagnetic resonance (EPR) spectroscopy was conducted according to previously described methods with some modifications (Paffett et al. 2015). Following serum treatment, mCECs were incubated with the iron-chelate NO-spin trap Fe2+-di(N-methyl-D-glutaminedithiocarbamate) (Fe2+(MGD)2; 1mM, final concentration) for 5 min. The iron-chelator Fe2+(MGD)2 was freshly prepared by mixing a stock solution of ferrous sulfate (FeSO4; 20 mM, dissolved in deionized water under N2) and an equal volume of sodium N-methyl-D-glucamine dithiocarbamate (NaMGD; 100 mM, dissolved in deionized water under N2) to give a molar ratio of 1:5, respectively, prior to each experiment. Following the incubation period, the incubation medium (400 µL) containing spin trapped NO was immediately transferred into custom-made gas permeable Teflon tubing (Zeus Industries, Raritan, NJ), folded four times, and inserted into a quartz EPR tube open at each end. The quartz EPR tube was inserted within the cavity of a Bruker EleXsys E540 X-band EPR spectrometer (Billerica, MA) operating at 9.8 GHz and 100 kHz field modulation and spectra was recorded after spectrometer tuning at room temperature. The EPR spectrum of spin trapped-NO were acquired from untreated mCECs with a scan time of 40s, and 10 scans were obtained and averaged to produce significant signal-to-noise ratio. EPR measurements from mCECs stimulated with 2 mM ATP to induce NO release were performed under the same conditions. Instrument settings were as follows: magnetic field, 3440 G; scan range, 100 G; microwave power, 21 mW; modulation frequency, 100 kHz; modulation amplitude, 1.0 G; time constant, 20 ms. The EPR spectra were collected, stored, and manipulated using the Bruker Software Xepr (Billerica, MA). NO levels were quantified and peak-to-peak measurements were taken and expressed in relative units.

mCECs were grown to confluence on six-well plates and incubated with 10% MWCNT exposed serum for 4 h. Following serum treatment, mCECs were incubated with Fe2+(MGD)2. Following application of the trap, a supernatant sample was isolated and NO was measured to assess a baseline reading. NO generation at baseline was negligible. Endothelial cells were subsequently stimulated with 2 mM adenosine triphosphate (ATP) for 5 min, followed by measurement of NO in a second supernatant sample.

2.5 *Ex vivo* vascular function using myography

Rings from the thoracic aorta were isolated and cleaned of connective tissue. Segments of aorta (2 mm length) were mounted in a 4-chamber myograph (610M; Danish Myo Technology A/S, Aarhus, Denmark). Vessels were submerged in physiological saline solution (composition in millimolar: 119.0 NaCl, 25.0 NaHCO3, 5.5 glucose, 4.7 KCl, 1.2 MgSO4, 1.2 KH2PO4, 0.025 EDTA, 2.5 CaCl2) bubbled at 37°C with 21% O2-5% CO2 balance N2 and left to equilibrate for 30 min. Tension was applied in 2 mN stepwise increments over 30 min to an optimal passive tension of 9 mN. Preliminary experiments showed that this tension produced optimal contraction and relaxation responses. Data from force transducers were processed by a MacLab/4e A-DI converter displayed through LabChart software (AD Instruments).

Vessel viability was confirmed by a contractile response to the addition of potassium containing physiological salt solution (KPSS in millimolar: 64.9 NaCl, 25.0 NaHCO3, 5.5 glucose, 58.9 KCl, 1.2 MgSO4, 1.2 KH2PO4, 0.025 EDTA, 2.5 CaCl2) repeated twice. Aortic rings isolated from naïve C57BL/6J or CD36-null mice were mounted in a myograph and challenged twice with KPSS as described above. After a 30-min equilibration period, vessels were incubated with 1% serum that was collected from mice exposed to dispersion media or MWCNT. Because the addition of serum induced contraction of aortic rings, the cumulative concentration-response curves to ACh (10-9-10-4) were acquired only after the response to serum had stabilized.

2.6 Matrix Metalloproteinase Protein Levels in Lung

Lung lavage fluid and whole lung homogenates were assayed for MMP-2 and MMP-9 protein concentrations using enzyme-linked immunoassay kits according to manufacturer's instructions (Boster, Pleasanton, CA).

2.7 Blood Brain Barrier Permeability

Animals were injected with 2% fluorescein sodium salt (Sigma-Aldrich F6377-100g, lot # MKBR1855V) 1 hour prior to sacrifice. Animals were transcardially perfused with ice cold saline prior to removal and dissection of the brain. Animals received Fasudil HCl (Selleckchem Catalog # S1573) formulated at 20mg/kg 2 hours before sacrifice. Brains were weighed and homogenized in 500µl of 50% trichloroacetic acid. Following homogenization, supernatants were neutralized with 400µl of 5M sodium hydroxide. Neutralized homogenate was spun down for 10 minutes at 10,000g to pellet the tissue. A 200µl sample was placed in a 96 well optical bottom plate (Nalgene Nunc International lot # 1019415) and read at 525/440nm in a spectrofluorophotometer.

2.8 Immunohistochemistry

Four animals from each group were anesthetized with isoflurane and transcardially perfused with saline followed by ice cold paraformaldehyde (PFA, 4% in PBS, pH 7.4). Brains were removed by decapitation, placed overnight in 4% PFA at 4°C, and then transferred to a 30% sucrose solution for ~48 hours at 4°C. Following cryoprotection, samples were rinsed with PBS and frozen in optimal cutting temperature compound. 16 µm sagittal sections were collected on a cryostat, dried, and stored at -20°C until use.

Sections were blocked and permeabilized with a PBS solution containing 1% bovine serum albumin, 5% goat serum, and 0.2% Triton X-100 for two hours at room temperature (RT). Primary antibodies were applied overnight at 4°C and were either rabbit anti-glial fibrillary acidic protein (GFAP, 1:500, Dako, Z0334) to label astrocytes, or rabbit anti-platelet endothelial cell adhesion molecule (PECAM-1, 1:100, Santa Cruz Biotechnology, sc-1506-R) to visualize cerebral blood vessels. The secondary antibody used was a donkey anti-rabbit Alexa Fluor 555 (1:1000, Life Technologies, A31572) and was applied for 2 hours at RT. All sections were stained with 4',6-diamidino-2-phenylindole (DAPI, 1:1000, Life Technologies, D3571) to label cell nuclei.

Imaging was performed by a blinded researcher on a Nikon TE2000 microscope with a Nuance spectral camera (Quorum, model #N-MSI-FX) in the University of New Mexico Fluorescence Microscopy Shared Resource Center. Astrocytes were imaged in the hippocampus and cerebellar regions at 20X, and GFAP intensity was quantified as a marker of astrocyte activation using ImageJ software (NIH). In the cerebellum, three separate images were taken randomly throughout lobule regions and GFAP intensity was averaged. Cerebellar vasculature and fluorescein permeation were visualized using a 40X objective oil immersion lens.

2.9 Tissue relative mRNA expression:

RNA was isolated from frozen lung (left lobe) and liver using the RNeasy Mini Kit (Qiagen, Valencia, CA, USA). Evaluation of gene expression was determined by standard 96-well technology using the StepOne™ (Applied Biosystems, Carlsbad, CA, USA) with pre-designed Assays-on-Demand™ TaqMan® probes and primers (Applied Biosystems). For lung *Il6* (Mn00446190_m1), *Ccl2* (Mn00441242_m1), and *Cxcl2* (Mn00436450_m1) were measured. For liver *Mt1* (Mn00496660_g1), *Mt2* (Mn00809556_s1), *Saa1* (Mn00656927_g1), *Hp* (Mn00516884_m1), and *Apcs* (Mn00488099_g1) were measured. Using 96 well plates, one µg of total RNA was reverse transcribed using random hexamers (Applied Biosystems) and Superscript III (Invitrogen, Carlsbad, CA). Nine µl of cDNA (1/10) was then used for gene expression determination. Hypoxanthine-guanine phosphoribosyltransferase was used as an internal reference. Relative gene expression was calculated using the comparative threshold method ($2^{-\Delta\Delta Ct}$) with vehicle-treated mice serving as the reference group (Livak and Schmittgen 2001).

2.10 Biometric analysis.

Labeled cRNA, from an input RNA of 375 ng, was prepared according to the manufacturer's protocol, using the illumina TotalPrep RNA Amplification Kit (Ambion, Catalog #IL1791) for hybridization to the arrays. The labeled cRNA samples were then assessed for quality and quantity. To ensure consistency for the array hybridization, all cRNA samples for each time point were quantified at the same time. The illumina RatRef-12 beadchip contains 22,523 probes and allows twelve samples to be interrogated in parallel. After a 20 h hybridization period at 58°C, the beadchips were scanned using an Illumina BeadStation 500G - BeadArray Reader (Illumina, Inc., San Diego, CA, USA).

2.11 Cell Culture.

Mouse Cerebrovascular Endothelial Cells (MCECs) were obtained from a commercial vendor (Cell Biologics) and maintained according to manufactures recommendations at 37° and 5% CO_2 – 95% O_2 with complete endothelial cell medium supplemented with 10% Fetal Bovine Serum (FBS). All experiments were performed between passages 3-8. Upon final plating, approximately $2*10^4$ cells were added to each well of a 24-well plate (Beckon Dickinson) and grown to confluence to mimic the cell-cell environment found in the vasculature. Cells were serum starved for 12 hours prior to treatment with serum. Assays were batched by exposure to enhance consistency and comparability across samples.

2.12 Serum-treated MCECs.

For the volume limited MWCNT exposure samples, exposed serum was added to the wells at a ratio of 1:9 (10%) with basal endothelial cell medium. Exposed serum was added in a similar manner from dispersion media controls in a 1:9 (10%). There was no FBS when exposed serum was mixed with basal endothelial cell medium. All treatments were done for 4 hours.

2.13 Microarray Analysis

Total RNA was extracted from cultured endothelial cells and purified with Qiagen RNeasy kit from each sample (Qiagen, Valencia, CA). The total RNA concentrations were measured using the NanoDrop ND-1000 (ThermoScientific, Wilmington, DE), and RNA integrity was checked using Agilent 2100Bioanalyzer to assure sufficient quality before proceeding with microarray hybridization.

Affymetrix GeneChip Mouse 430 2.0 arrays were used for gene expression analysis. All procedures were performed according to the manufactures instructions (Affymetrix, Santa Clara, CA). Briefly, 1.0µg of total RNA was used to generate double-stranded complementary DNA (cDNA) using an oligo dT-primer containing the T7 RNA polymerase promoter site and One-Cycle Target Labeling Kit (Affymetrix). cDNA was purified via column purifications using the GeneChip Sample Cleanup Module (Affymetrix), and biotinylated complementary RNA (cRNA) was synthesized by in vitro transcription using the GeneChip IVT Labeling Kit (Affymetrix). Biotin-labeled cRNA was purified and absorbance measured at 260 nm to determine yield (NanoDrop). Twenty micrograms of the labeled cRNA was fragmented and hybridized to the Affymetrix GeneChip Mouse 430 2.0 arrays for 16 h at 45_C following the Affymetrix protocol specific to the array type. Washing and staining were performed on the Affymetrix Fluidics 450 station according to the antibody amplification protocol (EukGE-Ws2v%;Fluidics Script). The GeneChips were scanned using the Affymetrix GeneChip Scanner 3000.

Statistical analysis procedures for whole microarray datasets have been extensively described (Erdely et al., 2014). Briefly, samples were imported into illumina® Beadstudio 3.0.19.0 and reference, hybridization control, stringency and negative control genes were checked for proper chip detection. Beadarray expression data were then exported with mean fluorescent intensity across like beads and bead variance estimates into flat files for subsequent analysis. Illumina BeadArray expression data were analyzed in Bioconductor using the ‘lumi’ and ‘limma’ packages. Gene lists containing group means of expression, p-values and standard fold changes were utilized as input for subsequent bioinformatics analysis. The Downstream Effects Analysis were generated through the use of Ingenuity Pathway Analysis (Ingenuity® Systems, www.ingenuity.com). Whole datasets

containing gene identifiers and corresponding expression values were uploaded into the application and a core analysis was done. Each identifier was mapped to its corresponding object in Ingenuity's Knowledge Base. In this study the following analysis criteria were utilized: log ratio of 0.5 and $p<0.01$. We have previously shown that a 1.1-1.3 fold change offered a reasonable number of molecules to evaluate responses (Erdely et al., 2014). The log ratio of 0.5 used in this study corresponds to a 1.4 fold change. The differentially expressed genes were evaluated by the Downstream Effects Analysis which enables a visualization of biological trends in the dataset and predict the effect of gene expression changes on biological processes and disease or on toxicological functions. The analysis identifies functions that are expected to increase or decrease, given the observed gene expression changes. The Downstream Effects Analysis is based on expected causal effects between genes and functions; the expected causal effects are derived from the literature compiled in the Ingenuity® Knowledge Base.

2.14 Flow Cytometry for Cell Surface Markers.

Following 4h serum treatment, MCECs were washed with PBS, trypsonized, and collected in 12x75mm culture tubes (VWR). MCECs were then incubated with primary antibody for either VCAM-1 (BD Biosciences, Lot #-2117560, FITC conjugate) or ICAM-1 (BD Biosciences, Lot #-25775, PE conjugate), washed 3x with PBS, and suspended in 3% BSA. Samples were read on a BD Biosciences LSRFortessa.

2.15 Cell Migration Assay

MCECs were plated on 8-well chamber slides and allowed to come to confluence. Cells were then scratched with a p200 pipette tip and washed with PBS before exposed serum was applied to the cells. Chambers were then placed in a live cell imaging system (Olympus) and a digital image was taken every 15 minutes for 6 hours. Cell area was quantified with ImageJ and plotted over time, represented as the average of 5-6 repetitions with unique animal sera per group.

2.16 Statistics

Myographic studies were compared with a two-way analysis of variance considering exposure and acetylcholine concentration as the two factors, and post-hoc comparisons at specific acetylcholine concentrations were conducted using Dunnett’s multiple comparisons test or Fisher’s least significant difference testing (GraphPad Prism, v 6.0). Other comparisons were conducted with a standard one-way or two-way ANOVA analysis of variance. $P<0.05$ was used as the limit of statistical significance.

3. RESULTS

3.1 MWCNT-7 Exposure results in Lung Cytotoxicity and Permeability Changes

MWCNT-7 used in the present study have been previously characterized (Porter et al. 2010). The average diameter was 49 nm with a mean length of 3.86 µm (geometric standard deviation = 1.94; **Figure 1A,B**). Purity was >99% carbon. Exposure to MWCNT-7 resulted in a dose-dependent increase in bronchoalveolar lavage (BAL) lactate dehydrogenase (LDH) activity at the 4 h time point, which also remained elevated at the 24 h time point. The 40 µg dose approximately doubled LDH levels compared to controls at both time points, with the 10 µg dose resulting in a 50% increase at both time points (**Figure 1C**). There was no significant difference in albumin levels between groups at the 4 h time point; however, both the 10 and 40 µg doses showed elevated albumin at the 24 h time point when compared to controls. (**Figure 1D**).

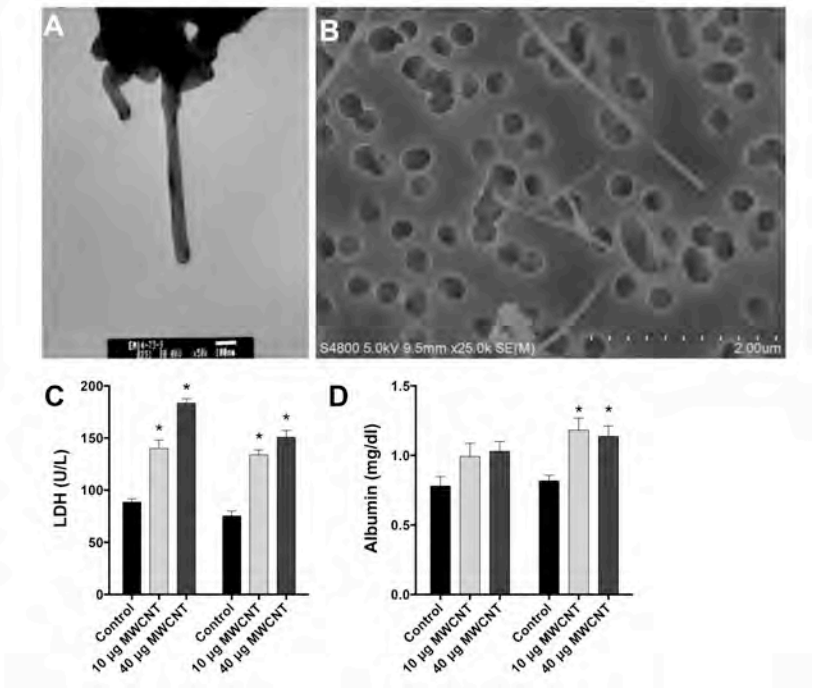

Figure 1. A,B. MWCNT-7 characterization by electron microscopy demonstrates the relative size and adequacy of dispersion. **C,D.** Markers of injury in the lung lavage, LDH and albumin levels, were increased following exposure (*p<0.05 vs DM by ANOVA, N=4-8 per group).

3.2 Pulmonary Delivery of MWCNT Drives Lung and Systemic Transcriptional Responses

Representative transmission and scanning electron microscopy images of the MWCNT demonstrates the relative size and adequacy of dispersion (**Figure 2**). Following exposure to MWCNT multiple markers of inflammation were increased 10-15 fold in the lungs including systemic pro-inflammatory markers *Il6* and *Ccl2*, as well as *Cxcl2*; a chemokine secreted by macrophages that acts as a chemoattractant for neutrophils and stem cells (**Figure 2**). These effects persisted at 24 h in a primarily dose dependent manner.

Following exposure there was a 40-80 fold increase of liver enzyme gene expression, indicative of an acute inflammatory phase response. All responses were dose dependent with the 40µg dose eliciting a particularly strong response (**Figure 2**). Responses were elevated at both time points, however by the 24hr mark expression levels had significantly decreased when compared to 4hrs.

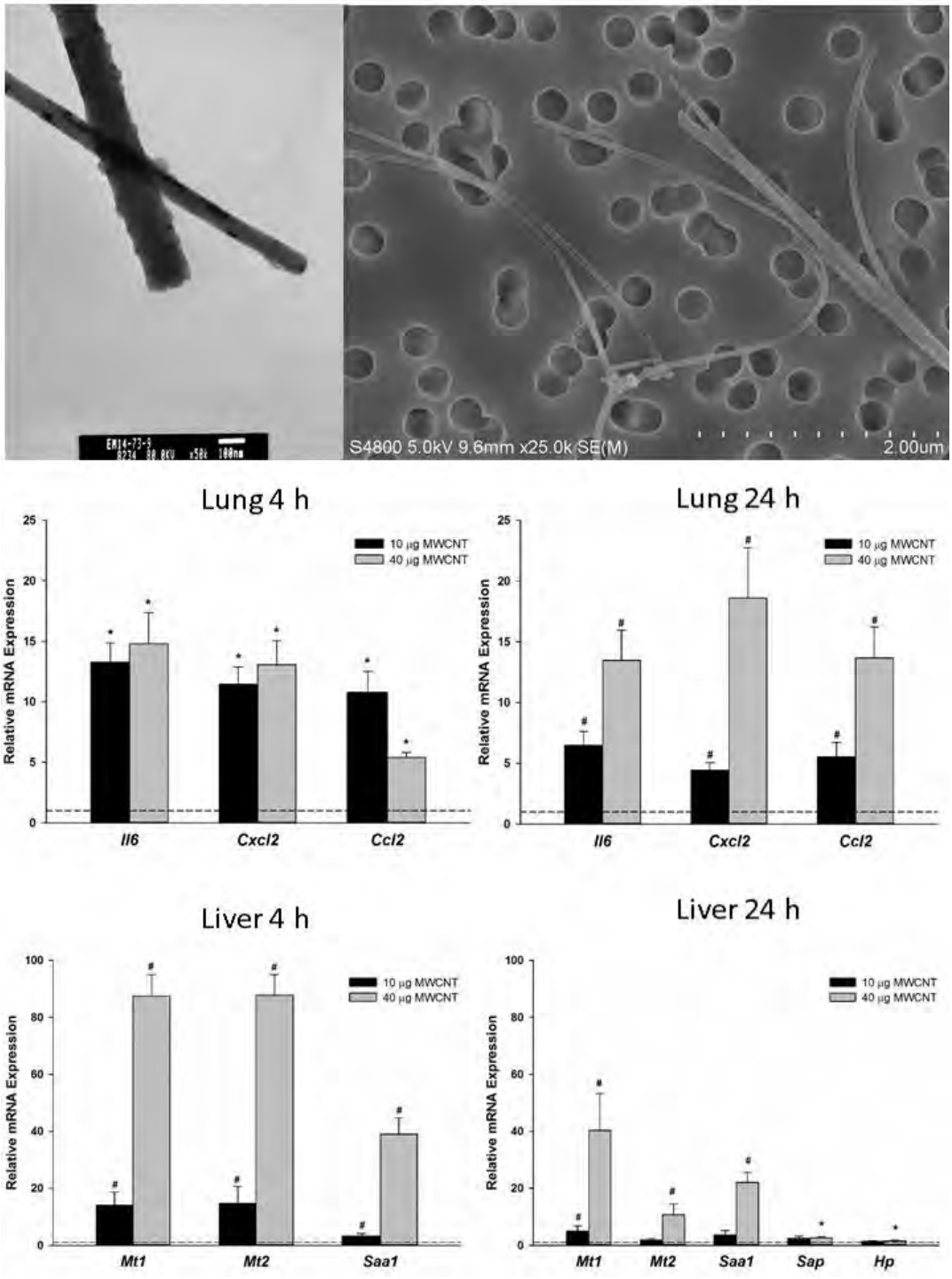

Figure 2. MWCNT-7 characterization by electron microscopy demonstrates the relative size and adequacy of dispersion. Markers of injury in the lung and liver were increased at 4 and 24h following exposure. ($^{\#}p<0.05$ vs all groups; *$p<0.05$ vs DM, N=6 per group).

3.3 Serum from MWCNT-Exposed Mice Decreases Endothelial NO Generation In Vitro

The supernatant of serum-treated endothelial cells, when treated with ATP and the NO spin-trap MGD, afforded a strong signal detectable by electron paramagnetic resonance spectroscopy (**Figure 3A**). Baseline measurements of unstimulated endothelial cells resulted in negligible amounts of NO production between groups treated with exposed or control serum. In ATP-stimulated cells, however,

serum from MWCNT-7-exposed mice decreased NO bioavailability by 30% when compared to cells incubated with serum from DM control mice (**Figure 3B**).

These results led us to speculate that the serum from MWCNT-7-exposed mice was able to directly affect eNOS or that the serum had the capacity to “scavenge” produced NO. To address this question we applied an acellular assay, bypassing the contribution of eNOS. MGD in iron-free media was incubated with serum from MWCNT-exposed mice and the NO-donor spermine NONOate (1M) as in previous studies with serum from ozone-exposed rodents (Paffett et al. 2015). However, serum from MWCNT-7-exposed mice had no effect on NO bioavailability when compared to serum from control mice (**Figure 3C**). These results suggested that serum from MWCNT-7-exposed mice diminishes eNOS generation of NO, rather than NO bioavailability.

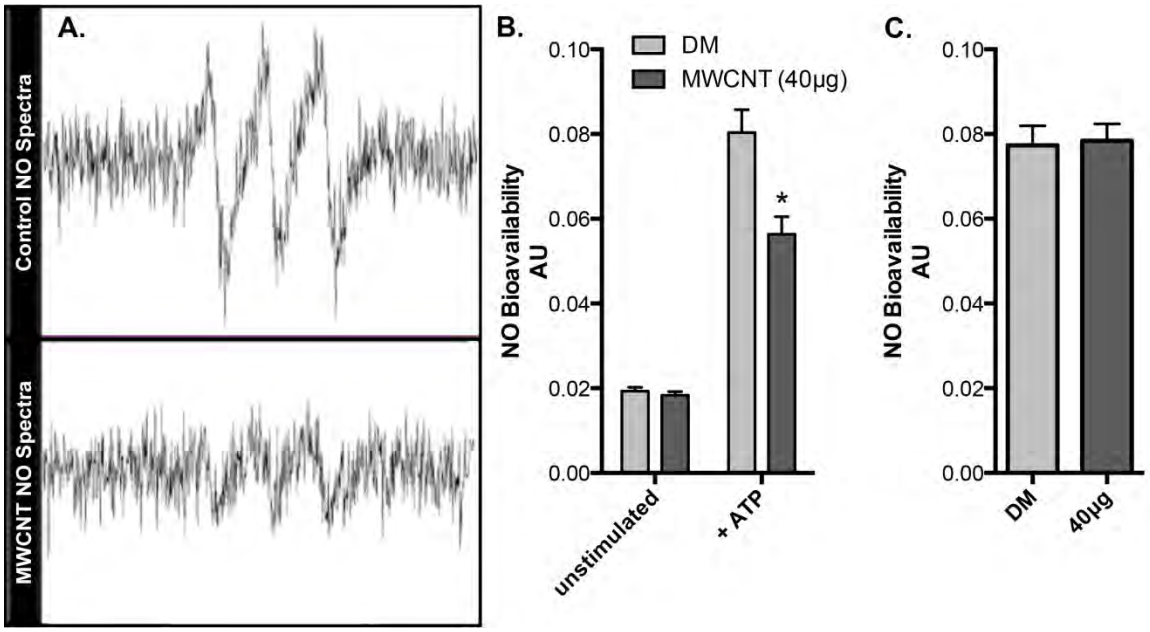

Figure 3. Effects of serum from MWCNT-7-exposed mice on NO generation and bioavailabilty.

A. Representative EPR spectra from endothelial cells incubated with control serum and serum from MWCNT-7-exposed mice. **B.** Unstimulated endothelial cells exhibited minimal baseline levels of detectable NO, which was not different when incubated with serum from DM (control) or MWCNT-7-treated mice. However, when stimulated by ATP, endothelial cells incubated with control serum demonstrated a significantly greater capacity to generate NO than cells treated with serum from MWCNT-7-exposed mice (*$p<0.05$, N=3 per group). **C.** In an acellular assay, levels of NO in iron-free media containing a known concentration of the NO donor, spermine NONOate, were not different in the presence of serum from control or MWCNT-7-treated mice.

3.4 Serum from MWCNT-7-Exposed Mice Diminishes Vasorelaxation Ex Vivo

We next examined the role that MWCNT exposure might have in a functional physiological system. We employed force-transduction myography with an isolated aortic ring preparation to test the serum bioactivity. Serum from both doses of MWCNT-7-exposed mice was able to significantly reduce acetylcholine (ACh)-induced relaxation (**Figure 4**). Interestingly, the serum from 10 µg-treated mice collected 4 h post-exposure (**Figure 4A**) was more potent in terms of inhibiting relaxation than was serum from 40 µg-treated mice, with the lower dose reaching a maximum relaxation of only 13.6%, compared to 27.1% for the higher dose and 49.4% for vehicle controls. This effect persisted at least 24 h post-exposure (**Figure 4B**), although more variability was noted. At 24 h post exposure, serum

from both low and high dose groups similarly inhibited relaxation (26.9% and 28.5%, respectively), as compared to DM control serum.

In addition to ACh responses, we assessed whether the initial contraction induced by serum treatment was similar between groups. Maximum vessel constriction induced by serum was measured and normalized to a potassium physiological saline solution (KPSS) response. There were no differences between control and MWCNT doses at 4 h with complete serum (**Figure 4A right panel**). However, serum obtained 24 h following MWCNT exposure did induce a modest but significantly higher average constriction in the 40 µg group (101% vs 80% for the low dose and 87% for the control; **Figure 4B right panel**).

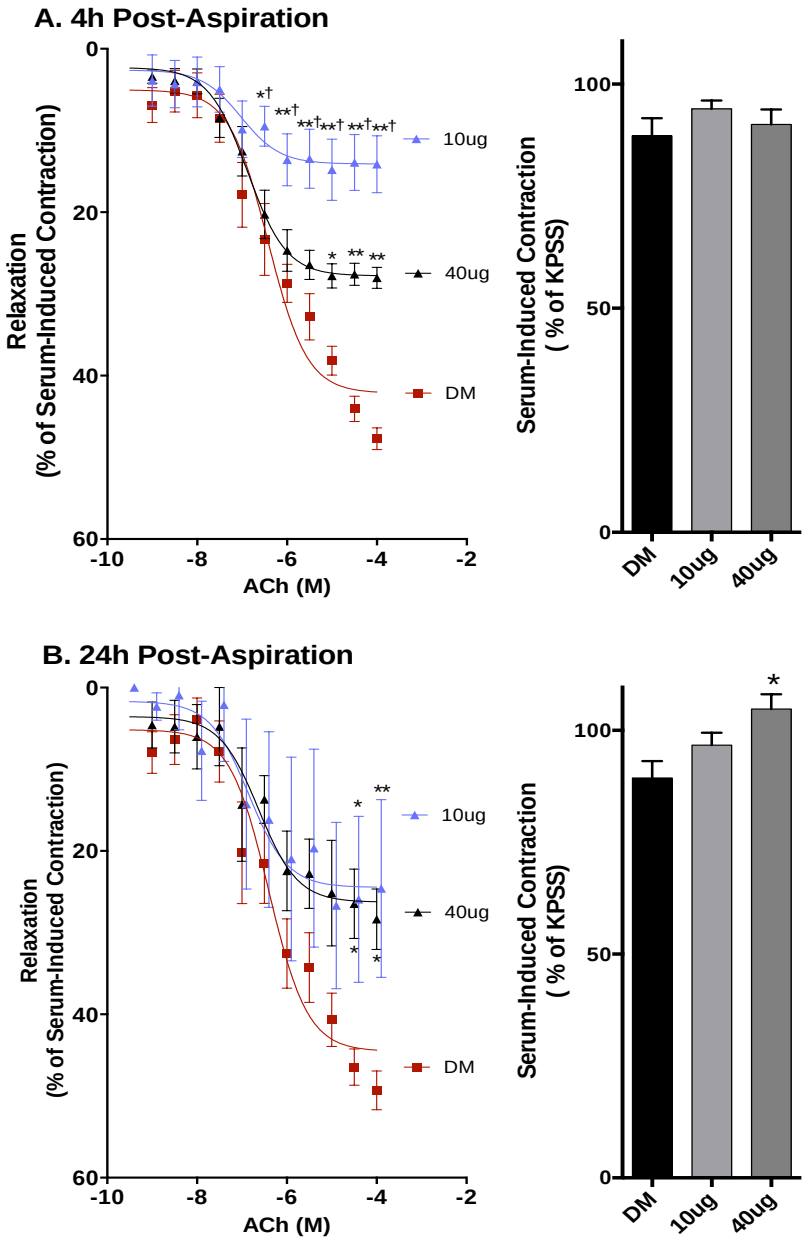

Figure 4. Myographic Effects of Serum from MWCNT-7-Exposed Mice.

A. Mouse serum obtained 4 h following MWCNT-7 treatment inhibited ACh-mediated vasorelaxation in aortic rings from untreated (naïve) mice (left) and maximum vessel constriction induced by serum (normalized to a KPSS response; right). Interestingly, the serum from low dose-treated mice was more potent than serum from high dose-treated mice. Asterisks indicates significant difference from control by two-way ANOVA with Tukey's multiple comparison test (*p<0.05,

P<0.001), dagger represents significant difference between the 10 and 40 µg doses (†p<0.01; N=10 per group). **B. Mouse serum obtained 24 h following MWCNT-7 treatment inhibited ACh-mediated vasorelaxation in aortic rings from untreated (naïve) mice (left), however the increased potency of the low dose exposure at 4 h was no longer observed. Maximum vessel constriction induced by serum (normalized to a KPSS response) is also shown (right of each relaxation curve). *Indicates significant difference from DM control by two-way ANOVA (*p<0.05, **P<0.01; N=6−8 per group).

3.5 Impact of Serum Fractionation on Vasorelaxation Responses

As an initial attempt to understand how serum bioactivity is driven by altered biochemistry and to exclude a direct nanomaterial effect on vasorelaxation, the serum was filtered to resolve smaller components (< 10 kDa) for aortic ring treatments. Notably, the filtered serum allowed for greater overall relaxation to ACh compared to whole serum, with an average relaxation of 77.39% for aortic rings incubated with filtered serum from DM-treated mice. In the 4 h post-exposure samples, the <10 kDa biomolecules induced a prominent anti-relaxation effect of serum from both doses of MWCNT-7-exposed mice, although the specific enhanced potency of the 10 µg dose was no longer observed (Figure 3.4A). The anti-relaxant effect of filtered serum components from MWCNT-7-treated mice was largely abolished in the 24 h post-exposure serum (**Figure 5B**), suggesting that the <10 kDa biomolecules may have complexed with larger biomolecules or that larger biomolecules contribute to a persistent effect. There were no differences in initial contraction between control and MWCNT doses with 4 h filtered serum (removal of large, >10 kD proteins), or with 24 h filtered serum (**Figure 5A,B right panels**, respectively).

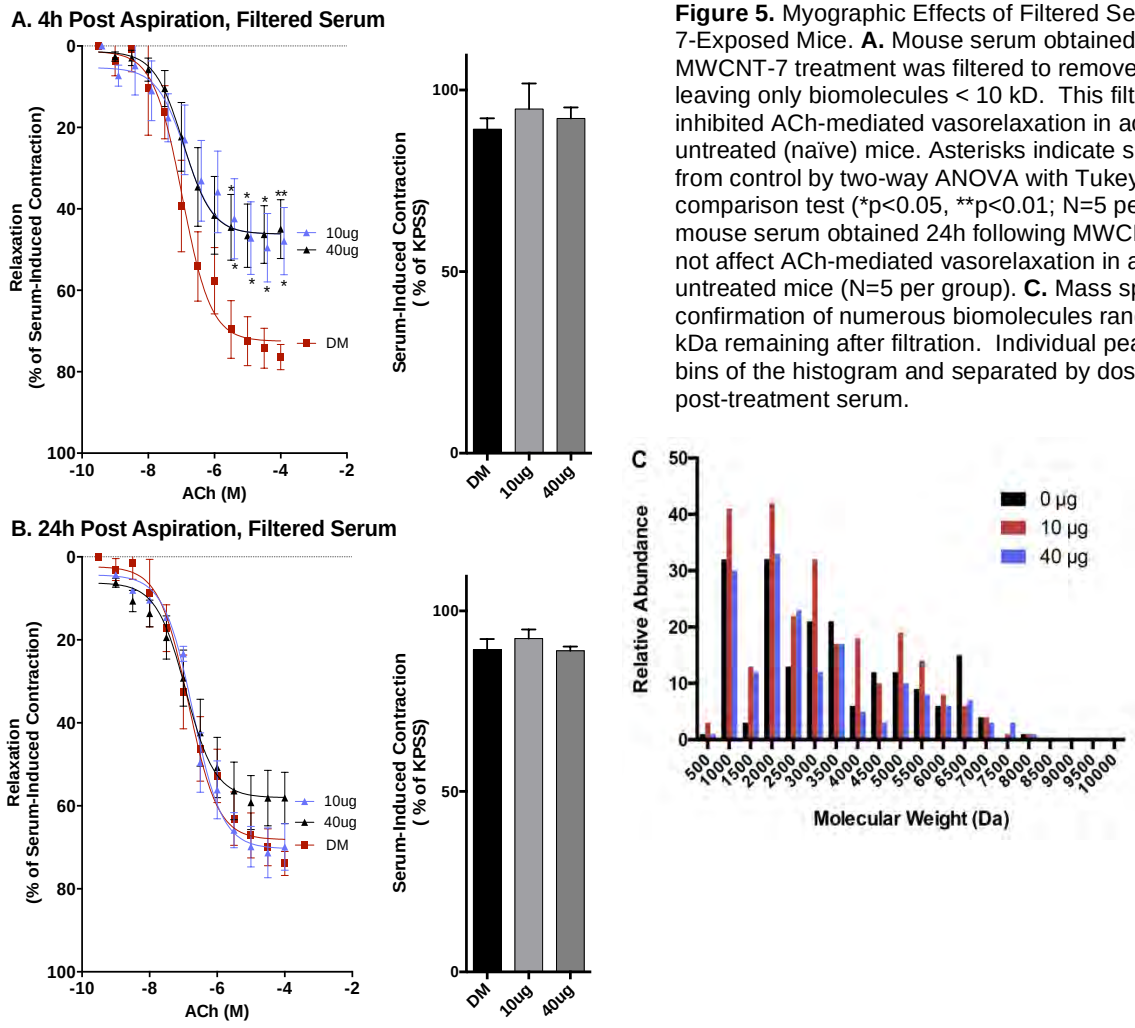

Figure 5. Myographic Effects of Filtered Serum from MWCNT-7-Exposed Mice. **A.** Mouse serum obtained 4 h following MWCNT-7 treatment was filtered to remove all larger proteins, leaving only biomolecules < 10 kD. This filtered serum still inhibited ACh-mediated vasorelaxation in aortic rings from untreated (naïve) mice. Asterisks indicate significant difference from control by two-way ANOVA with Tukey's multiple comparison test (*p<0.05, **p<0.01; N=5 per group). **B.** Filtered mouse serum obtained 24h following MWCNT-7 treatment did not affect ACh-mediated vasorelaxation in aortic rings from untreated mice (N=5 per group). **C.** Mass spectroscopic confirmation of numerous biomolecules ranging from 0.5 – 10 kDa remaining after filtration. Individual peaks are collected into bins of the histogram and separated by dose group for the 4 h post-treatment serum.

We employed LC/MSMS analysis to confirm that the serum fraction consisted of biomolecules below 10 kDa (**Figure 5C**). Further, in comparing the < 10 kDa serum fraction between treatment groups, we resolved differences in the mass distribution among doses, consistent with the observations of nonlinear dose effects. Importantly, findings with filtered sera demonstrate that bioactivity can be induced without any possibility of direct nanomaterial or leukocyte interaction with the endothelium.

3.6 Vascular CD36 Mediates Endothelial Dysfunction Induced by Serum from MWCNT-7-Exposed Mice

Aortas harvested from CD36-null mice were employed to determine if the scavenger-receptor mediated effects of serum from MWCNT-7-exposed mice were similar to previous findings with ozone and ambient PM (Rao et al. 2014; Robertson et al. 2013). CD36-null aortic relaxation in response to ACh was not impacted by serum from MWCNT-7-exposed mice compared to serum from control mice (**Figure 6**). All three groups reached an average maximum relaxation of ~50% (comparable to WT vessels), with no discernible differences between the groups at either time point. These results denote that the bioactive compounds in the serum following MWCNT-7 exposure interact with CD36 to impair vasorelaxation.

Interestingly, however, serum from MWCNT-7-exposed mice applied to CD36-/- vessels was observed to

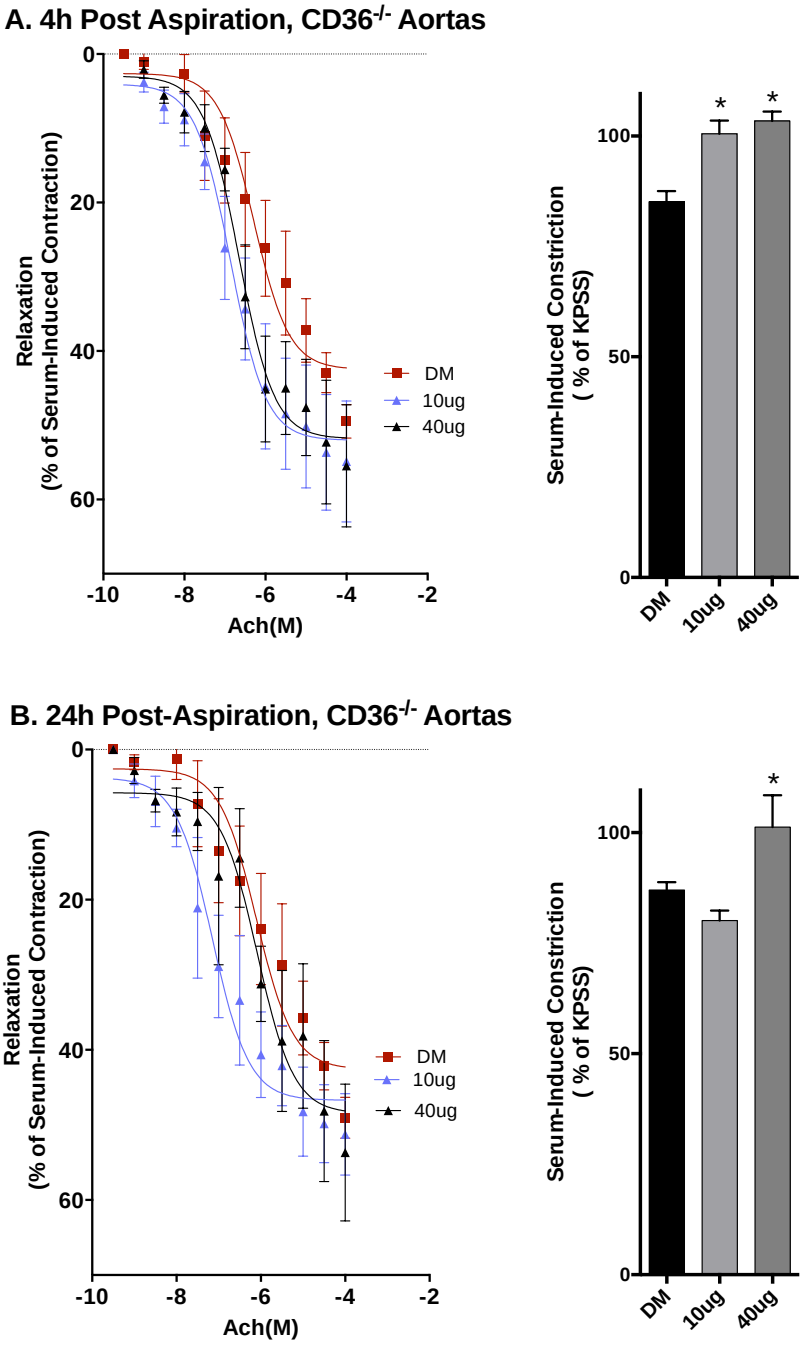

Figure 6. CD36 Role in Vascular Response to MWCNT-Induced Serum Factors.

A. Mouse serum obtained 4 h following MWCNT-7 treatment had no effect on ACh-mediated vasorelaxation in aortic rings from untreated CD36-null mice (N=5 per group). Significant differences in the contractile response to the serum addition was noted for serum from MWCNT-7-treated mice. Asterisks indicate significant difference from control by ANOVA with Dunnett's multiple comparison test (*p<0.05; n=5 per group). **B.** Filtered mouse serum obtained 24 h following MWCNT-7 treatment had no effect on ACh-mediated vasorelaxation in aortic rings from untreated CD36-null mice (N=4−5 per group). Significant differences in the contractile response to the serum addition was noted for serum from the 40 µg MWCNT-7-treated mice. Asterisks indicate significant difference from control by ANOVA with Dunnett's multiple comparison test (*p<0.05; n=5 per group).

induce a greater average contraction of 100% for the lower and 104% for the higher dose group at the 4 h mark compared to aortic rings treated with control serum (87%; **Figure 6A, right panel**). By 24 h, the high dose group achieved a contraction of 101%, while the low dose was not different from controls (**Figure 6B, right panel**). These findings contrast with the vasorelaxation data in that CD36 is not required to induce contraction due to MWCNT-induced, serum-borne components.

3.7 Serum from MMP-9 Deficient Mice Exhibits Reduced Vascular Bioactivity after MWCNT-7 Exposure

Lastly, we investigated the potential role of MMP-9 as a source of circulating ligands that are generated as a result of MWCNT-7 exposure. MMP-9 levels in WT mice treated with 10 and 40 µg MWCNT-7 were measured in the lung and BAL at the protein level. MMP-9 was up regulated in the BAL at both 10 and 40 µg doses at 4h, and in the 40 µg dose at 24h (**Figure 7A and B**). MMP-9 was also significantly upregulated in the lung lysate in the 40 µg dose at 24h (**Figure 7D**). In contrast, MMP-2 protein levels were unchanged in the lung lavage (Supplemental Figure 1).

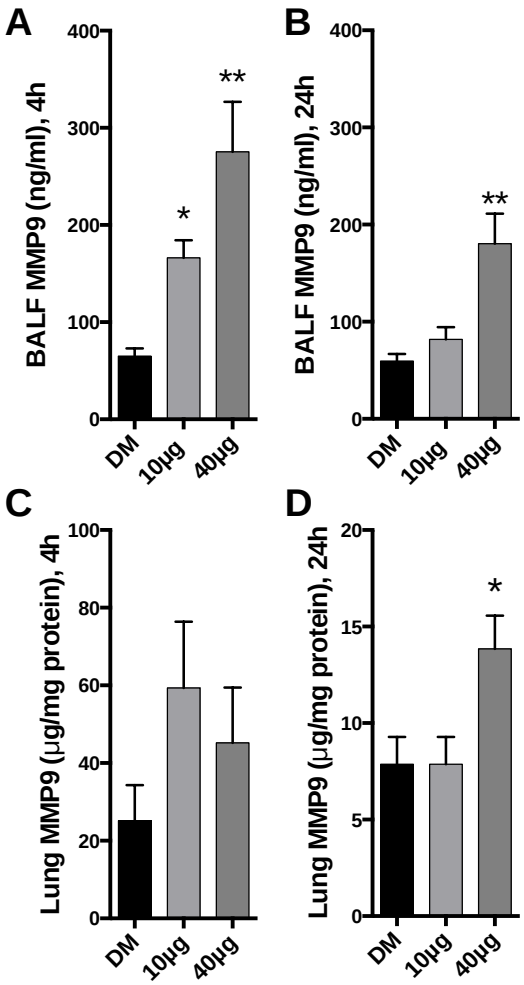

Figure 7. MMP-9 protein levels in bronchoalveolar lavage **(**A,B**)** and whole lung lysates (C,D) from MWCNT-7-exposed mice. Asterisks indicate significant difference from control by ANOVA with Dunnett's multiple comparison test (*p<0.05; **p<0.01).

Building on the finding of MWCNT-7-induced pulmonary MMP-9 expression, MMP-9-/- mice were exposed to MWCNT-7 and the bioactivity of the serum was tested for its ability to affect eNOS mediated vasorelaxation ex vivo. Deficiency of MMP-9 (**Figure 8**) appeared fully protective relative to WT outcomes (**Figure 4**). Pulmonary MWCNT-7 cytotoxicity, as measured by LDH activity in the BALF, was similar between both WT and MMP9-/- mice (**Figure 8A**). In both dose groups, WT vessels treated with serum from MMP-9-/- mice achieved similar maximal relaxation compared with serum from DM-treated MMP-9-/- mice, with an average response of ~55% (**Figure 8B**). However, the dose-response curve revealed a significant right-shift in both dose groups relative to DM-control serum, which suggests that some residual bioactivity may be derived outside of MMP-9 activity. DM-control serum from the MMP-9-/- mice was actually more permissive of vasorelaxation that WT serum in this ex vivo assay, which further adds to the conjecture that MMP-9-derived degradation products may impair vascular function (Supplemental Figure 2). Serum-mediated constriction (**Figure 8C**) was unaltered between exposure groups in the MMP-9-/- animals. Collective maximal vasorelaxation outcomes for each permutation at the 4-h time point clearly show that pulmonary MWCNT-7 exposure leads to bioactivity in the serum that impairs vasorelaxation in a manner dependent on MMP-9 to generate the signal and CD36 to respond (Supplemental Figure 3).

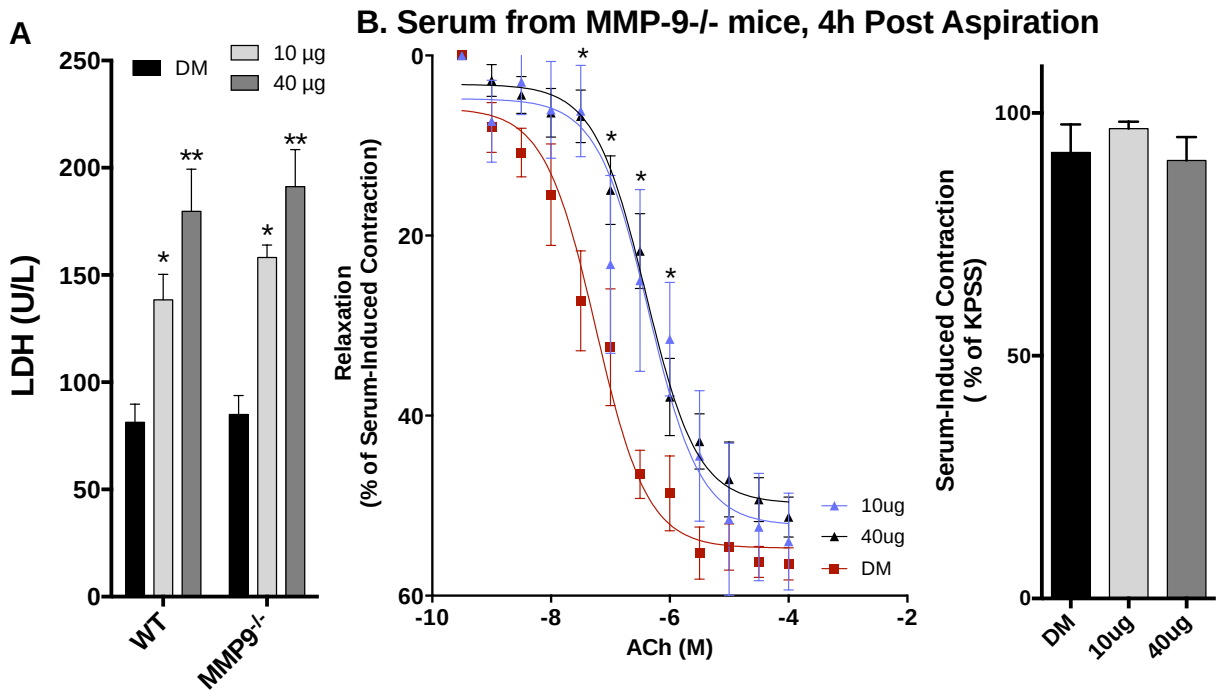

Figure 8. Myographic Effects of Serum from MWCNT-7-Exposed MMP-9$^{-/-}$ Mice

A. MMP-9$^{-/-}$ mice exhibit similar degree of lung injury at 4 h post MWCNT-7 aspiration, as measured by LDH from the BALF. Asterisks indicate significant difference from control by two-way ANOVA with Tukey's multiple comparison test (*p<0.01; **p<0.001). **B.** Serum from MMP-9$^{-/-}$ mice treated with 10 or 40 µg MWCNT-7 caused a modest right-shift effect on the concentration response to ACh-mediated vasorelaxation in WT vessels, compared to serum from the DM control mice, but did not reduce the overall magnitude of relaxation. Serum from the various groups exhibited a consistent contractile effect on all aortas. Asterisks indicate significant difference from control by two-way ANOVA with Tukey's multiple comparison test (*p<0.05; n=5-6 per group).

3.8 Evidence of BBB Disruption and Neuroinflammation Following MWCNT Exposure

Immunohistochemistry of the cerebellum and hippocampus in mice 4h post-exposure to MWCNT revealed elevated GFAP staining, indicative of activated astrocytes, compared with DM-exposed control mice (**Figure 9**). Microglia were present, as indicated by IBA-1 staining, but were morphologically inactive (Supplemental figure 1). PECAM labeling of blood vessels identified fluorescein leaking in the animals that had been exposed to MWCNTs compared to DM-exposed controls. (**Figure 9**)

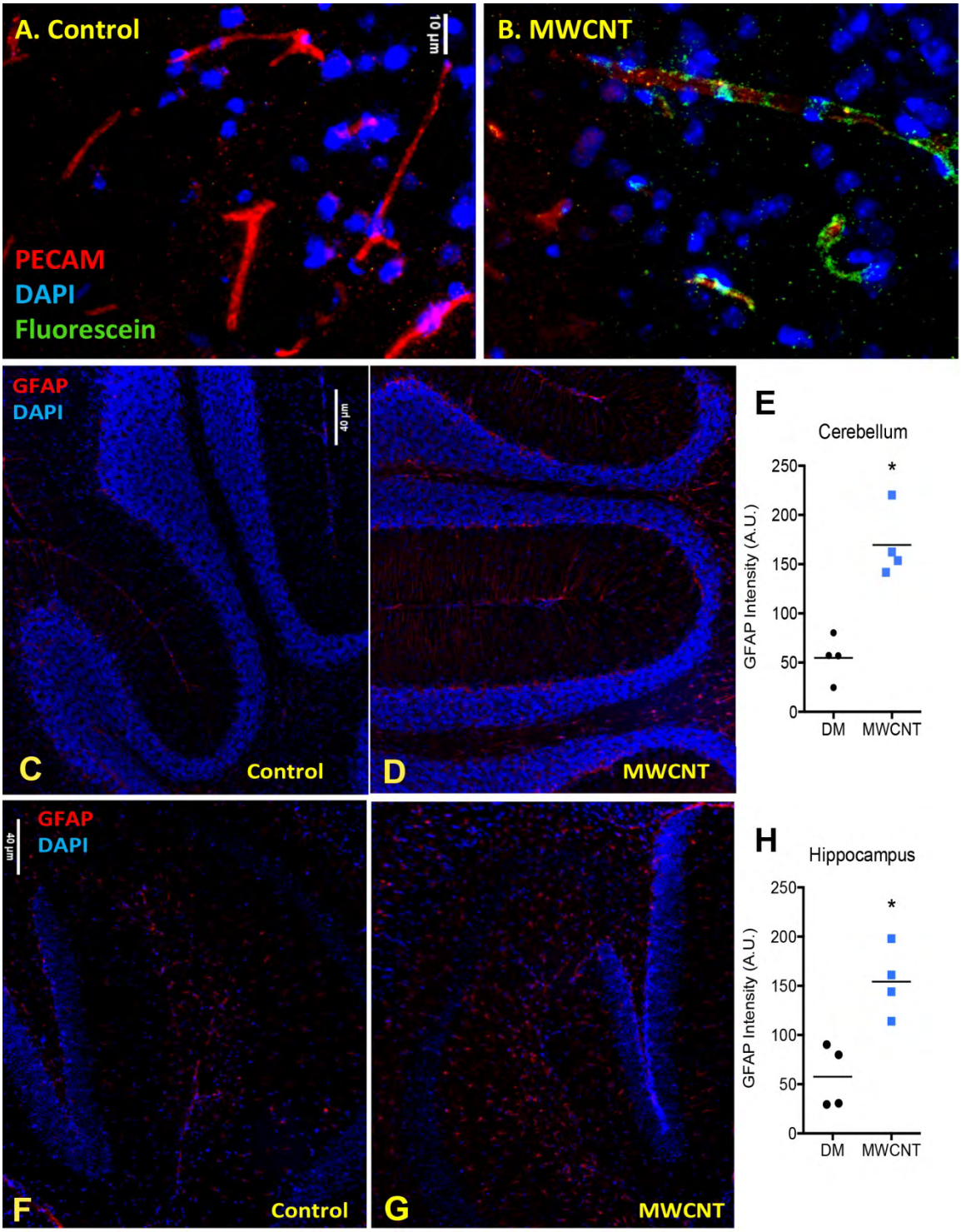

Figure 9. MWCNT (10 µg) exposure acutely induces inflammatory responses in the brain. Figures A-B, fluorescein in the brain of exposed mice versus vehicle controls. Figures C-H visualization and quantification of astrocyte activation in the cerebellum and hippocampus. * indicates a p value of <0.05 by students t test.

3.9 Dependence of MWCNT-Induced Neuroinflammation on BBB Disruption

To specifically delineate whether the neuroinflammation was the result of loss of BBB integrity, mice were administered vehicle or the rho kinase inhibitor fasudil, which has been shown to improve BBB function and improve outcomes in stroke-related models (Gibson et al. 2014; Satoh et al. 1996). Mice received fasudil either 2h after MWCNT aspiration, but before injection of the BBB tracer sodium

fluorescein, or prior to MWCNT and again 2 hours later. The former permutation was designed to see if fluorescein uptake in the brain could be inhibited after exposure and neuroinflammation had occurred. The latter permutation was to prevent BBB disruption throughout the time course to test whether neuroinflammatory changes still occurred in the absence of BBB disruption.

Fluorescein uptake in the brain was significantly enhanced 4h after exposure to MWCNT (**Figure 10**). This pulmonary exposure was associated with increased Il6 and CcL5 mRNA expression in cortical regions, and increased CcL5 mRNA in the hippocampus (**Figure 10**). Treatment with fasudil at 2h post-exposure completely blocked fluorescein uptake in the brain, but had no effect on brain inflammatory outcomes.

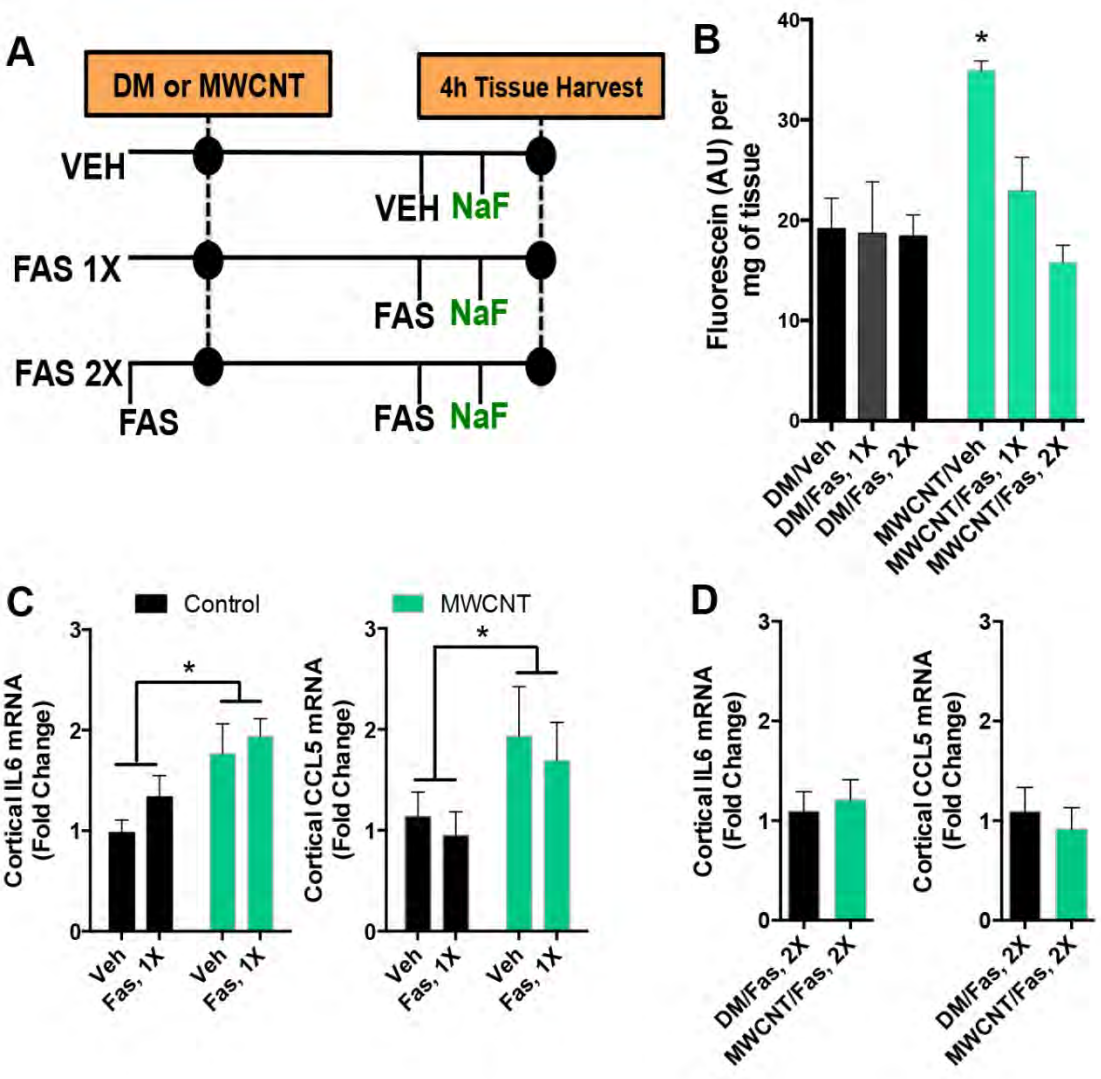

Figure 10. MWCNT-induced neuroinflammatory responses are dependent on BBB disruption.

A. General study design, incorporating a single (1X) fasudil treatment after MWCNT to reduce brain fluorescein uptake and a preventative (2X) fasudil treatment to prevent MWCNT-induced BBB disruption throughout the 4h timecourse. **B**. Fluorescein uptake in brains 4h following MWCNT aspiration with vehicle, 1X or 2X fasudil treatment. Asterisk indicates significant difference from control by ANOVA ($P<0.05$). **C**. Inflammatory markers IL-6, CCL5 mRNA in the cortex 4h following DM or MWCNT aspiration. Asterisks indicate a significant effect of MWCNT compared to control in a 2-way ANOVA ($P<0.05$) with no influence of the single post-MWCNT fasudil treatment. **D**. Preventative (2X) fasudil administration abrogated inflammatory marker mRNA expression (IL-6, CCL5) in the cortex.

3.10 Dependence of MWCNT induced Neuroinflammation dependent on BBB disruption

CD36 is a class II scavenger receptor involved in a wide range processes including fatty acid metabolism(Hajri et al. 2002), heart disease, and atherosclerosis(Febbraio et al. 2000). CD36$^{-/-}$ mice showed no increases in fluorescein or pro-inflammatory gene expression in the cortex or hippocampus 4h following 10µg MWCNT aspiration. **(Figure 11)**

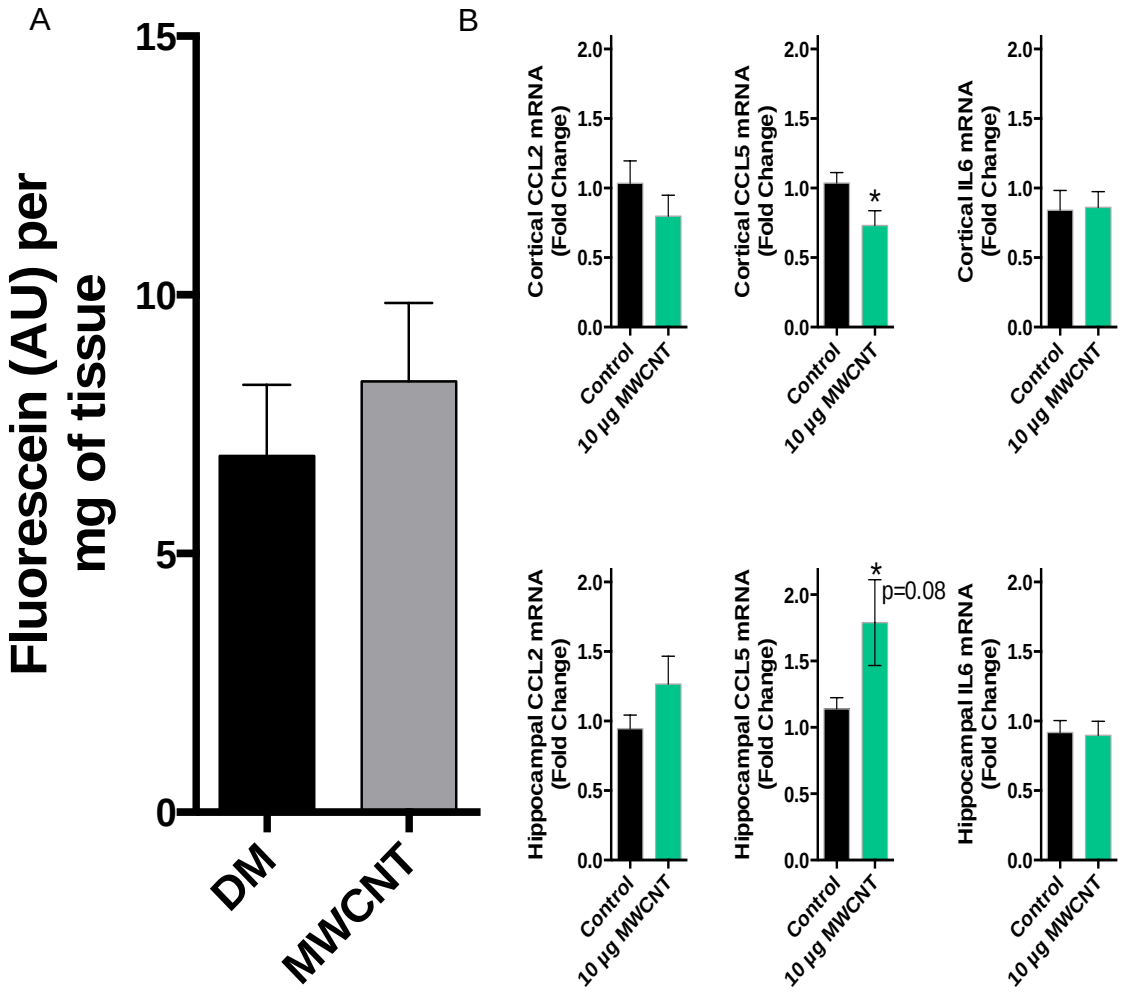

Figure 11. CD36 mice are largely protected from the BBB disruption and neuroinflammatory effects of pulmonary MWCNT exposure. **A.** Fluorescein uptake in the brain of CD36$^{-/-}$ mice 4h following treatment with DM or MWCNT. **B.** Neuroinflammatory markers in the cortex and hippocampus of CD36$^{-/-}$.

3.11 Bioactivity of MWCNT-Induced, Serum-Borne Factors: Endothelial Inflammatory Responses

Microarray analysis was performed on mRNA isolated from endothelial cells after they had been treated with serum collected from MWCNT-exposed serum. The results of the microarray revealed induced disease or functional categories associated with inflammation, immune response, and chemoattraction / recruitment of leukocytes. The effect was more prominent in endothelial cells challenged with serum collected from mice exposed to 40 µg MWCNT. (**Figure 12**).

Application of 10% serum from MWCNT-treated mice on primary murine cerebrovascular endothelial cells for 4h resulted in a 50% increase in vascular cell adhesion molecule-1 (Vcam-1) and

approximately 3-fold increases in relative mRNA expression of C-C motif ligand-2 (Ccl-2) and C-C motif ligand-5 (Ccl-5) pro-inflammatory cytokines in the 40µg dose at the 4hr tim12e point (**Figure 12A-C**). The 10µg caused slight increases in Ccl-2 and Ccl-5, but was not statistically significant.

Similarly, treatment of primary murine cerebrovascular endothelial cells with serum from MWCNT-treated mice elicited small, but significant up-regulation of both VCAM-1 and intercellular adhesion molecule-1 (ICAM-1) on the cell surface, as assessed by flow cytometry (**Figure 12D,E**). By 24hrs the effects had returned to baseline. These data taken in conjunction with the gene expression are consistent with activation of the endothelium via canonical NFkB intracellular signaling pathways.

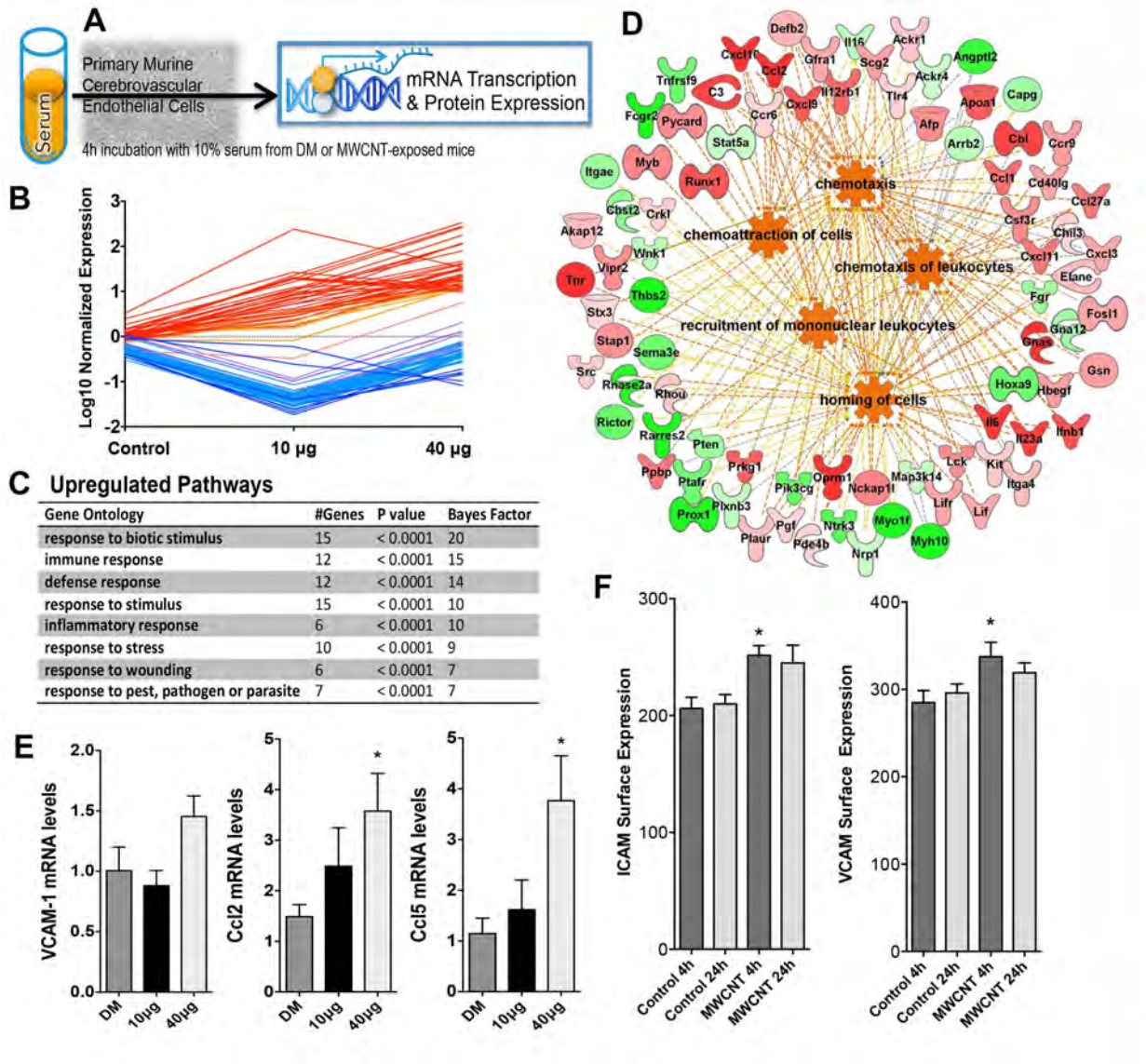

Gene Ontology	#Genes	P value	Bayes Factor
response to biotic stimulus	15	< 0.0001	20
immune response	12	< 0.0001	15
defense response	12	< 0.0001	14
response to stimulus	15	< 0.0001	10
inflammatory response	6	< 0.0001	10
response to stress	10	< 0.0001	9
response to wounding	6	< 0.0001	7
response to pest, pathogen or parasite	7	< 0.0001	7

Figure 12. Inflammatory responses of cerebrovascular endothelial cells treated with serum from MWCNT-exposed mice.

A. General depiction of assay protocol, with serum from exposed mice incubated on primary murine cerebrovascular endothelial cells. **B**. Microarray results indicate numerous transcripts (60) from serum-treated endothelial cells were elevated in a dose-dependent manner; elevated transcripts were ontologically related inflammatory and/or cellular defense response. **C**. Specific inflammatory genes responses from microarray results. **D**. Gene ontology graphs showing the relationships between up-regulated inflammatory genes. **E**. Confirmation of key inflammatory mRNA responses by PCR finds that endothelial VCAM-1, Ccl-2, and Ccl-5 mRNA were all significantly up regulated by serum from MWCNT-treated mice. **F.** Endothelial cell surface ICAM-1 and VCAM-1 protein expression were both elevated by serum from mice exposed to the 40µg dose of MWCNT as compared to control. Asterisks denote significant difference from DM control serum ($P<0.05$).

3.12 Bioactivity of MWCNT-Induced, Serum-Borne Factors: Endothelial Cell Regrowth and Motility

A scratch assay was employed to assess the functional effects of serum collected from MWCNT-exposed serum. Serum was applied to confluent endothelial cells that had been “scratched” with a sterile pipette tip and allowed to grow back over the course of 6 h. During the regrowth, images were taken every 15 minutes and total cell area was quantified. At the 6 h mark, the controls had achieved 100 µm of cell growth when compared to 60 µm of growth for the 40 µg group and 50 µm of growth for the 10µg group. (**Figure 13**) These results were in complement to the microarray results indicating significantly decreased gene expression related to cell cycle, mitosis, and cytokinesis which was more prevalent in endothelial cells incubated with serum collected from mice exposed to 10 µg of MWCNT (**Figure 13**).

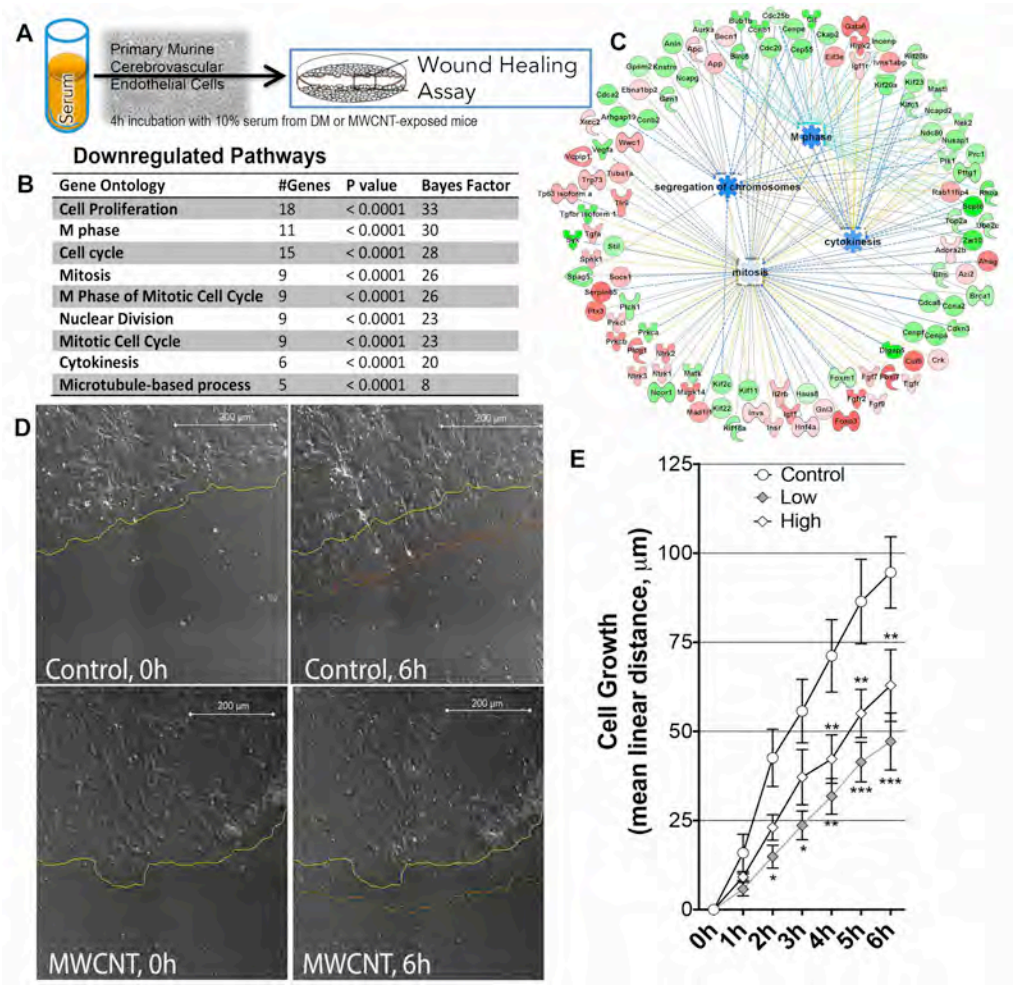

Figure 13. Serum from MWCNT-exposed mice inhibits endothelial cell growth and motility.

A. General depiction of assay protocol, with serum from exposed mice incubated on primary murine cerebrovascular endothelial cells. **B.** Ontological classifications of 86 significantly down regulated genes (noted in Figure 4.5B) suggest loss of cell motility and growth pathways. **C**. Gene ontology charts showing the relationship between genes that are down regulated **D**. Live cell images of wound recovery, showing the initial edge of endothelial cells (yellow dashed line) and the edge after 6 h (orange dashed line). **E**. Mean cell regrowth following wounding in primary cerebrovascular endothelial cells incubated with serum from DM or MWCNT-exposed mice. Asterisks denote significant difference from DM control serum effects using a 2-way Repeated Measures ANOVA (*P<0.05; **P<0.01; ***P<0.001).

4. DISCUSSION

In these studies we provide functional evidence for a mechanism by which MWCNT-7 exerts systemic endothelial dysfunction and inflammation, which appears to be indirectly mediated by serum-borne components. Pulmonary exposure to MWCNT-7 led to the generation of bioactive factors in the serum that significantly impaired vascular function ex vivo and drove inflammatory and cellular defense mechanisms in vitro. The principal components of the serum that confer abnormal vasorelaxation and neuroinflammation act at least in part through the vascular CD36 scavenger receptor and appear, at least acutely (4 h) in vasorelaxation studies, to involve smaller biomolecules (<10 kDa) released into circulation. The vasoactivity effects of MWCNT-7-induced serum biomolecules were not linearly associated with lung burden and may reflect induction of different biological responses at different doses.

Within these studies, we have utilized this endothelial cell biosensor paradigm to outline a plausible anatomical/physiological pathway by which 1) ligands are derived from MMP-9 activity in the lung, 2) access the circulation and 3) interact with vascular CD36 receptors to impair vasorelaxation and induce neuroinflammation. This overarching paradigm provides concrete mechanistic detail to theories of pulmonary “spillover” that explain the pathogenesis of extrapulmonary effects of inhaled particulates (Brook et al. 2010; Van Eeden et al. 2012), although the biological complexity with potentially numerous metalloproteinases and pattern recognition receptors involved must be considered. Importantly, the observed vascular effects with serum from mice exposed to MWCNT-7 by a pulmonary route resolves issues inherent to direct-application nanomaterial research with cells or organs, offering an alternative and more anatomically sound approach to study mechanisms underlying the extrapulmonary toxicity of inhaled particulates.

Isolated Vascular Studies

The mechanism by which serum from MWCNT-7-exposed mice exerts its effects on vascular relaxation presumably involves impairment of eNOS and NO generation. Inhalation of pollutants such as diesel emissions can lead to uncoupling of eNOS and similar loss of dilatory function (Cherng et al. 2011; Knuckles et al. 2008). Nurkiewicz et al. found that TiO2 nanoparticles could directly scavenge NO (Nurkiewicz et al. 2009), an effect that was eliminated in the presence of antioxidants. We recently observed that serum from ozone-exposed rats exhibited diminished serum levels of nitrites and nitrates, and there was some evidence for increased nitrosothiol formation in serum, suggesting that NO scavenging may occur (Paffett et al. 2015). In the present study, however, serum from MWCNT-7-exposed mice inhibited aortic vasorelaxation and endothelial cell generation of NO, but did not scavenge spermine NONOate-donated NO. The outcomes from cell culture and isolated aortic rings suggest that a ligand-receptor interaction, and resultant intracellular signaling, mediated a loss of eNOS activity and diminished vasorelaxation.

One potential mechanism to explain how serum from MWCNT-7-exposed mice could impair eNOS is through the generation of CD36-interacting ligands (Uittenbogaard et al. 2000). Specific ligands to CD36 can adversely affect the lipid composition of caveole, interfering with eNOS and potentially causing eNOS to become uncoupled (Fleming et al. 2005; Shaul 2003; Wong et al. 2011). The present data, combined with recent studies of ozone-induced endothelial dysfunction (Robertson et al. 2013), implicate an important role for CD36 in mediating the loss of aortic vasorelaxation caused

by serum from MWCNT-7-treated mice. Notably, vessel relaxation in CD36-null aortas was more robust than in WT aortas when treated with control serum. CD36 has been implicated as a key inflammatory mediator in response to particulate matter exposure, an important component of the macrophage response to oxidized lipids (Rao et al. 2014) and thus may have broader implications for extrapulmonary effects than just endothelial dysfunction.

We propose that an additional crucial step required for the induction of eNOS-compromising bioactivity in serum from MWCNT-7-exposed mice involves the activation of pulmonary MMP-9, leading to the generation of protein fragments that can effect biological activity. MMP-9 plays a major role in the degradation of extracellular matrix in a large spectrum of physiological and pathophysiological process (Bekes et al. 2011). MMP-9 is secreted by a wide number of cell types including neutrophils, macrophages and fibroblasts, creating the potential for a large amount of MMP-9 to be generated as a result of lung injury. Exposures to gasoline engine emissions in mice led to system-wide changes in MMP-9 concentrations and activity, including induction within atherosclerotic plaques (Lund et al. 2009). Furthermore, serum MMP-9 was found to be elevated in both mice and humans exposed to diesel emissions (Lund et al. 2009). Pulmonary MMP-9 expression has also been associated with vanadium (Colin-Barenque et al. 2008), a vanadium-laden particulate (Su et al. 2000) and metal fume (Palmer et al. 2006) exposures. Few studies have examined the pathophysiological implications of MMP-9 activity in mediating pulmonary or extrapulmonary outcomes of inhaled particulates. Our study found that despite comparable acute (4-h) lung injury from MWCNT-7 exposure in WT and MMP-9-/- mice, MMP-9 deficiency resulted in diminished serum bioactivity after MWCNT-7 treatment compared to WT. Interestingly, serum from MMP-9 deficient mice treated with vehicle allowed for greater relaxation in aortic rings than did WT serum. MMP-9 has been shown to generate numerous vasoactive by-products from the degradation of extracellular matrix proteins, such as angiostatin (Cornelius et al. 1998; Pozzi et al. 2000), tumstatin (Hamano et al. 2003), and β-dystroglycan (Agrawal et al. 2006). MMP-9 may therefore be responsible for the generation of a number of vasoactive agents that help set baseline vascular tone.

Our study highlights the importance of pulmonary nanoparticle delivery in driving systemic vascular effects and the doses used in this study, based on numerous dosimetry analyses, represent an extreme but plausible scenario. It should be appreciated that more pronounced effects were achieved at lower depositions and a 1:100 dilution of serum from exposed mice nearly abolished vascular relaxation. Mice have a blood volume of approximately 2 mL, depending on their body weight. Even if all of the MWCNT-7 left the lungs and stayed in the bloodstream – a gross exaggeration – the MWCNT-7 concentration in serum would be approximately 5 µg/mL, which would then be further diluted in the vascular bath to a maximal theoretical (yet still improbably high) concentration of 50 ng/mL, a concentration far below what has been reported to induce endothelial cell toxicity in vitro. The rationale for this extreme estimation of dose lies in how pulmonary exposure to particulates leads to a clear systemic vascular toxicity that cannot be reproduced with direct exposures of particles to the vessels. Furthermore, filtration of serum which would exclude molecules >10 kDa and certainly any trace of MWCNT-7, did not entirely abrogate vascular effects. Studies employing an oral gavage of carbon black were unable to induce substantial vascular dysfunction in rats (Folkmann et al. 2012), and studies using an intravenous injection of diesel exhaust particles, at similar concentrations to the current MWCNT-7 doses, in mice were unable to induce vascular dysfunction (Bai and van Eeden

2013). The lack of biological effect in these alternate exposure routes serves to highlight the importance of the pulmonary exposure in the pathogenesis of vascular outcomes.

Blood Brain Barrier and Neuroinflammation Studies

Neurological effects of inhaled particulates have been reported but considerable uncertainty exists regarding the pathway by which toxic effects transfer from the lung to the brain. The present study establishes that a circulating signal arises after pulmonary exposure to MWCNT that leads to a BBB-dependent neuroinflammatory response. Serum from MWCNT-exposed mice upregulated adhesion molecules and pro-inflammatory cytokines in primary cerebrovascular endothelial cells at both the gene and protein level. Serum from exposed mice also adversely affected the ability of endothelial cells to migrate in a wound-healing assay. Collectively, these findings implicate a modified serum composition stemming from pulmonary interactions with MWCNT as a source of diminished BBB integrity and neural effects.

Severe disruption of BBB integrity has been documented in major cerebrovascular events or neurological diseases, and BBB permeability has been directly linked to neuroinflammation. Ischemia/Reperfusion in spontaneously hypertensive rats has been associated with increased BBB permeability (Aoki et al. 2002). MRI imaging showed increased BBB permeability in people with multiple sclerosis (Cramer et al. 2014). Mouse models of Alzheimer's disease have found BBB permeability to precede the formation of the β-amyloid plaques that are the hallmark of the disease(Ujiie et al. 2003).

Rho kinase inhibition has been shown to reduce neuropathology in scenarios where BBB is otherwise dysfunctional. Fasudil treatment in a mouse ischemia model was found to prevent BBB permeability as well as the formation of oxidative stress(Gibson et al. 2014). Rho kinase inhibition with fasudil has been shown to accelerate functional recovery in different mouse and rat spinal cord injury models, with fasudil given locally or systemically after injury(Dergham et al. 2002; Fournier et al. 2003; Hara et al. 2000). Autoimmune demyelinating disorders, such as multiple sclerosis, have been treated with Rho kinase inhibitors with great success. It is thought that Rho kinase inhibition in these disorders prevents the leukocyte migration into the central nervous system(Walters et al. 2002).

The class B scavenger receptor CD36 mediates free radical production and brain injury in cerebral ischemia(Ueno et al. 2011). It has also been shown to activate the Rho/Rho kinase pathway(Wraith et al. 2013). Our lab has found CD36 to play a key role in mediating vasorelaxation as a result of ozone exposure(Robertson et al. 2013). Loss of CD36 prevented both the BBB permeability and neuroinflammation that was associated with MWCNT exposure, suggesting an important role for CD36 activation.

Inhalation of PM has been associated with neuroinflammation and BBB integrity deficits (Campbell et al. 2009; Gerlofs-Nijland et al. 2010), but this is the first study to show a mechanistic link between the two outcomes. Oppenheim et al identified significant increases in brain fluorescein uptake resulting from long-term exposure (50d) to a mixture of gasoline and diesel emissions in $ApoE^{-/-}$ mice (Oppenheim et al. 2013). These findings were similarly associated with increased cerebrovascular gelatinase levels and reduced occludin and claudin-5 expression and, in parallel, increased inducible nitric oxide synthase expression in the brain parenchyma. Rats exposed to diesel emissions for 6 months demonstrated significant increases in cortical TNFα, α-synuclein, and Aβ42 expression

(Levesque et al. 2011). Importantly, all of these studies involved long-term exposures, while the present study reveals effects within 4h of pulmonary MWCNT exposure.

Unique to this study is the idea that serum is able to drive disparate endothelial responses at multiple levels, consistent with a complex activation of multiple homeostatic responses at varying dose-response relationships. Due to the nature of the modifications in the serum there exists the possibility of activating multiple endothelial cell surface receptors, thereby eliciting a wide range of cellular responses. Our lab and others have shown that immunomodulatory scavenger receptors, such as CD36 (Rao et al. 2014; Robertson et al. 2013), TLR4 (Kampfrath et al. 2011), and LOX-1 (Lund et al. 2011) play a major role in eliciting endothelial inflammatory and antidilatory responses following exposure to various inhaled toxicants. Further study will be required to elucidate the principal ligand/receptor interactions responsible for activating the inflammatory responses.

Alternate pathways, such as direct delivery of inhaled particulates and CNTs have been hypothesized, but limited evidence exists demonstrating substantive transference of CNTs across the BBB, and no evidence for a direct biological effect has been mechanistically established in such studies. MWCNTs, specifically, accumulate in the brain in only small fractions of the original pulmonary dosage (0.001% of the lung burden at day 1 post-inhalation for 12 d), and specific confirmation that the material has penetrated beyond the capillary wall is often lacking in distribution studies, *i.e.,* much of the residual mass of CNTs may simply reside in the cerebrovascular compartment and not the brain tissue. CNTs, and specifically MWCNTs, have many characteristics that make them highly desirable as drug delivery platforms. The ability to withstand a high degree of functionalization is perhaps their most desirable feature. Many labs have employed MWCNTs as the basis for the targeted delivery of numerous compounds to different organs. MWCNTs were used to deliver Doxorubicin to brain glioma cells. The MWCNTs were PEGylated with angiopep-2 in BALB/c mice engrafted with C6 glioma cells. While the authors were able to discern a statistically significant amount of doxorubicin in the brain when compared to controls, they were unable to conclude that this route of delivery would be clinically relevant (Ren et al. 2012), despite extensive engineering efforts to target the brain (Kateb et al. 2007).

MWCNTs are able to withstand a high degree of functionalization, including surface coating, attachment of fluorescent linkers, and drug delivery insertion (Tsai et al. 2013). These manipulations are able to decrease the amount of toxicity that MWCNTs can induce (Vittorio et al. 2009), as well as allowing for less aggregation (Forati et al. 2011) and better clearance by the body (Bussy et al. 2015a). However targeting of CNTs to specific locations in the body is still very difficult (Mehra and Jain 2013; Peer et al. 2007; Ren et al. 2012). Targeting CNTs to the brain adds an extra layer of complexity when the BBB is taken into account. This specialized structure has proven to be especially adapt at keeping functionalized MWCNTs out of the brain (Kafa et al. 2015). Other labs have investigated both the *in vivo* biodistribution and pharmacokinetics of various permutations of drug delivery systems that were built on a MWCNT platform. Singh et al found that MWCNT-GEM complex with FA targeting in rats accumulated in major organs including the liver, lung, kidney and spleen(Singh et al. 2013). Moore et al investigated the biodistribution pattern of PLA-PEG-coated MWCNT loaded with PTX. Intravenously (IV) injected CNTs in mice showed accumulation in the lungs, liver, and spleen. These particular CNTs did show a lack of an inflammatory response when compared to controls(Wu et al. 2012).

Future analysis of the serum will be required to better understand the nature of the systemic effects that occur as a result of MWCNT exposure. While our proteomics data denotes a number of modified proteins following exposure (personal communication with Dr. Andrew Ottens), it is important to keep in mind that the analysis was only conducted on the fraction of the serum that was <5Kd, creating the possibility that larger proteins could also be affected. Lipidomic analysis could also provide information on the nature of the serum due to the potential for MWCNTs to interact with lipids in the lung.

Summary

In conclusion, serum obtained from mice exposed to MWCNT-7 has the capacity to impair vasorelaxation in naïve aortic rings ex vivo and induce neuroinflammation in vivo. Notably, the low dose of 10 µg induced even greater serum bioactivity at the 4-h time point for vasoactivity outcomes than did the 40 µg dose. Results from the present study further highlight the role of smaller, <10 kDa biomolecules, in addition to larger species, which appear to be generated by MMP-9 and may collectively act through the scavenger receptor CD36 to reduce responsiveness to ACh. These data further support the concept that pulmonary reactions lead to a spillover of secondary mediators from the lungs into the systemic circulation. Future work will need to further elucidate, via fractionation studies, which portions/components of the serum exhibit biological activity, as well as peptide sequencing to provide further insight into the enzymatic origins of the circulating peptides. Additionally, the use of serum from exposed mice in ex vivo assays offers a novel, more anatomically sophisticated and even translational approach for studying the systemic impact of inhaled substances.

REFERENCES

Agrawal S, Anderson P, Durbeej M, van Rooijen N, Ivars F, Opdenakker G, et al. 2006. Dystroglycan is selectively cleaved at the parenchymal basement membrane at sites of leukocyte extravasation in experimental autoimmune encephalomyelitis. J Exp Med 203:1007-1019.

Aird WC. 2008. Endothelium in health and disease. Pharmacological reports : PR 60:139-143.

Alheid U, Frolich JC, Forstermann U. 1987. Endothelium-derived relaxing factor from cultured human endothelial cells inhibits aggregation of human platelets. Thromb Res 47:561-571.

Aoki T, Sumii T, Mori T, Wang X, Lo EH. 2002. Blood-brain barrier disruption and matrix metalloproteinase-9 expression during reperfusion injury: Mechanical versus embolic focal ischemia in spontaneously hypertensive rats. Stroke 33:2711-2717.

Bai N, Khazaei M, van Eeden SF, Laher I. 2007. The pharmacology of particulate matter air pollution-induced cardiovascular dysfunction. Pharmacol Ther 113:16-29.

Bai N, van Eeden SF. 2013. Systemic and vascular effects of circulating diesel exhaust particulate matter. Inhal Toxicol 25:725-734.

Bekes EM, Schweighofer B, Kupriyanova TA, Zajac E, Ardi VC, Quigley JP, et al. 2011. Tumor-recruited neutrophils and neutrophil timp-free mmp-9 regulate coordinately the levels of tumor angiogenesis and efficiency of malignant cell intravasation. Am J Pathol 179:1455-1470.

Brook RD, Rajagopalan S, Pope CA, 3rd, Brook JR, Bhatnagar A, Diez-Roux AV, et al. 2010. Particulate matter air pollution and cardiovascular disease: An update to the scientific statement from the american heart association. Circulation 121:2331-2378.

Bussy C, Al-Jamal KT, Boczkowski J, Lanone S, Prato M, Bianco A, et al. 2015a. Microglia determine brain region-specific neurotoxic responses to chemically functionalized carbon nanotubes. ACS Nano 9:7815-7830.

Bussy C, Al-Jamal KT, Boczkowski J, Lanone S, Prato M, Bianco A, et al. 2015b. Microglia determine brain region-specific neurotoxic responses to chemically functionalized carbon nanotubes. ACS Nano.

Calderon-Garciduenas L, Reed W, Maronpot RR, Henriquez-Roldan C, Delgado-Chavez R, Calderon-Garciduenas A, et al. 2004. Brain inflammation and alzheimer's-like pathology in individuals exposed to severe air pollution. Toxicologic pathology 32:650-658.

Campbell A, Araujo JA, Li H, Sioutas C, Kleinman M. 2009. Particulate matter induced enhancement of inflammatory markers in the brains of apolipoprotein e knockout mice. J Nanosci Nanotechnol 9:5099-5104.

Cherng TW, Paffett ML, Jackson-Weaver O, Campen MJ, Walker BR, Kanagy NL. 2011. Mechanisms of diesel-induced endothelial nitric oxide synthase dysfunction in coronary arterioles. Environ Health Perspect 119:98-103.

Colin-Barenque L, Martinez-Hernandez MG, Baiza-Gutman LA, Avila-Costa MR, Ordonez-Librado JL, Bizarro-Nevares P, et al. 2008. Matrix metalloproteinases 2 and 9 in central nervous system and their modification after vanadium inhalation. J Appl Toxicol 28:718-723.

Cornelius LA, Nehring LC, Harding E, Bolanowski M, Welgus HG, Kobayashi DK, et al. 1998. Matrix metalloproteinases generate angiostatin: Effects on neovascularization. J Immunol 161:6845-6852.

Cramer SP, Simonsen H, Frederiksen JL, Rostrup E, Larsson HB. 2014. Abnormal blood-brain barrier permeability in normal appearing white matter in multiple sclerosis investigated by mri. Neuroimage Clin 4:182-189.

Dagouassat M, Lanone S, Boczkowski J. 2012. Interaction of matrix metalloproteinases with pulmonary pollutants. Eur Respir J 39:1021-1032.

Dergham P, Ellezam B, Essagian C, Avedissian H, Lubell WD, McKerracher L. 2002. Rho signaling pathway targeted to promote spinal cord repair. J Neurosci 22:6570-6577.

Distler U, Kuharev J, Navarro P, Levin Y, Schild H, Tenzer S. 2014. Drift time-specific collision energies enable deep-coverage data-independent acquisition proteomics. Nat Methods 11:167-170.

Erdely A, Hulderman T, Salmen R, Liston A, Zeidler-Erdely PC, Schwegler-Berry D, et al. 2009. Cross-talk between lung and systemic circulation during carbon nanotube respiratory exposure. Potential biomarkers. Nano letters 9:36-43.
Febbraio M, Abumrad NA, Hajjar DP, Sharma K, Cheng W, Pearce SF, et al. 1999. A null mutation in murine cd36 reveals an important role in fatty acid and lipoprotein metabolism. J Biol Chem 274:19055-19062.
Febbraio M, Podrez EA, Smith JD, Hajjar DP, Hazen SL, Hoff HF, et al. 2000. Targeted disruption of the class b scavenger receptor cd36 protects against atherosclerotic lesion development in mice. J Clin Invest 105:1049-1056.
Febbraio M, Hajjar DP, Silverstein RL. 2001. Cd36: A class b scavenger receptor involved in angiogenesis, atherosclerosis, inflammation, and lipid metabolism. J Clin Invest 108:785-791.
Fleming I, Mohamed A, Galle J, Turchanowa L, Brandes RP, Fisslthaler B, et al. 2005. Oxidized low-density lipoprotein increases superoxide production by endothelial nitric oxide synthase by inhibiting pkcalpha. Cardiovasc Res 65:897-906.
Folkmann JK, Vesterdal LK, Sheykhzade M, Loft S, Moller P. 2012. Endothelial dysfunction in normal and prediabetic rats with metabolic syndrome exposed by oral gavage to carbon black nanoparticles. Toxicol Sci 129:98-107.
Forati T, Behnamghader A, Rashidi A, Gozalian A, Ntentopolou D, Namvarasl M, et al. 2011. Effect of functionalized carbon nanotubes on the synthesis of hydroxyapatite nanoparticles. J Nanosci Nanotechnol 11:5423-5428.
Fournier AE, Takizawa BT, Strittmatter SM. 2003. Rho kinase inhibition enhances axonal regeneration in the injured cns. J Neurosci 23:1416-1423.
Fuller BF, Cortes DF, Landis MK, Yohannes H, Griffin HE, Stafflinger JE, et al. 2012. Exposure of rats to environmental tobacco smoke during cerebellar development alters behavior and perturbs mitochondrial energetics. Environ Health Perspect 120:1684-1691.
Gerlofs-Nijland ME, van Berlo D, Cassee FR, Schins RP, Wang K, Campbell A. 2010. Effect of prolonged exposure to diesel engine exhaust on proinflammatory markers in different regions of the rat brain. Particle and fibre toxicology 7:12.
Gibson CL, Srivastava K, Sprigg N, Bath PM, Bayraktutan U. 2014. Inhibition of rho-kinase protects cerebral barrier from ischaemia-evoked injury through modulations of endothelial cell oxidative stress and tight junctions. J Neurochem 129:816-826.
Hajri T, Han XX, Bonen A, Abumrad NA. 2002. Defective fatty acid uptake modulates insulin responsiveness and metabolic responses to diet in cd36-null mice. J Clin Invest 109:1381-1389.
Hamano Y, Zeisberg M, Sugimoto H, Lively JC, Maeshima Y, Yang C, et al. 2003. Physiological levels of tumstatin, a fragment of collagen iv alpha3 chain, are generated by mmp-9 proteolysis and suppress angiogenesis via alphav beta3 integrin. Cancer Cell 3:589-601.
Hara M, Takayasu M, Watanabe K, Noda A, Takagi T, Suzuki Y, et al. 2000. Protein kinase inhibition by fasudil hydrochloride promotes neurological recovery after spinal cord injury in rats. J Neurosurg 93:94-101.
Harrison DG. 1994. Endothelial dysfunction in atherosclerosis. Basic Res Cardiol 89 Suppl 1:87-102.
Kafa H, Wang JT, Rubio N, Venner K, Anderson G, Pach E, et al. 2015. The interaction of carbon nanotubes with an in vitro blood-brain barrier model and mouse brain in vivo. Biomaterials 53:437-452.
Kampfrath T, Maiseyeu A, Ying Z, Shah Z, Deiuliis JA, Xu X, et al. 2011. Chronic fine particulate matter exposure induces systemic vascular dysfunction via nadph oxidase and tlr4 pathways. Circ Res 108:716-726.
Kateb B, Van Handel M, Zhang L, Bronikowski MJ, Manohara H, Badie B. 2007. Internalization of mwcnts by microglia: Possible application in immunotherapy of brain tumors. Neuroimage 37 Suppl 1:S9-17.
Knuckles TL, Lund AK, Lucas SN, Campen MJ. 2008. Diesel exhaust exposure enhances venoconstriction via uncoupling of enos. Toxicol Appl Pharmacol 230:346-351.

Kubes P, Suzuki M, Granger DN. 1991. Nitric oxide: An endogenous modulator of leukocyte adhesion. Proc Natl Acad Sci U S A 88:4651-4655.
Kuharev J, Navarro P, Distler U, Jahn O, Tenzer S. 2014. In-depth evaluation of software tools for data-independent acquisition based label-free quantification. Proteomics.
Levesque S, Surace MJ, McDonald J, Block ML. 2011. Air pollution & the brain: Subchronic diesel exhaust exposure causes neuroinflammation and elevates early markers of neurodegenerative disease. J Neuroinflammation 8:105.
Li Z, Hulderman T, Salmen R, Chapman R, Leonard SS, Young SH, et al. 2007. Cardiovascular effects of pulmonary exposure to single-wall carbon nanotubes. Environ Health Perspect 115:377-382.
Livak KJ, Schmittgen TD. 2001. Analysis of relative gene expression data using real-time quantitative pcr and the 2(-delta delta c(t)) method. Methods 25:402-408.
Lund AK, Lucero J, Lucas S, Madden MC, McDonald JD, Seagrave JC, et al. 2009. Vehicular emissions induce vascular mmp-9 expression and activity associated with endothelin-1-mediated pathways. Arterioscler Thromb Vasc Biol 29:511-517.
Lund AK, Lucero J, Harman M, Madden MC, McDonald JD, Seagrave JC, et al. 2011. The oxidized low-density lipoprotein receptor mediates vascular effects of inhaled vehicle emissions. Am J Respir Crit Care Med 184:82-91.
Mehra NK, Jain NK. 2013. Development, characterization and cancer targeting potential of surface engineered carbon nanotubes. J Drug Target 21:745-758.
Mercer RR, Scabilloni JF, Hubbs AF, Wang L, Battelli LA, McKinney W, et al. 2013. Extrapulmonary transport of mwcnt following inhalation exposure. Particle and fibre toxicology 10:38.
Nunokawa Y, Tanaka S. 1992. Interferon-gamma inhibits proliferation of rat vascular smooth muscle cells by nitric oxide generation. Biochem Biophys Res Commun 188:409-415.
Nurkiewicz TR, Porter DW, Hubbs AF, Cumpston JL, Chen BT, Frazer DG, et al. 2008. Nanoparticle inhalation augments particle-dependent systemic microvascular dysfunction. Particle and fibre toxicology 5:1.
Nurkiewicz TR, Porter DW, Hubbs AF, Stone S, Chen BT, Frazer DG, et al. 2009. Pulmonary nanoparticle exposure disrupts systemic microvascular nitric oxide signaling. Toxicol Sci 110:191-203.
Oppenheim HA, Lucero J, Guyot AC, Herbert LM, McDonald JD, Mabondzo A, et al. 2013. Exposure to vehicle emissions results in altered blood brain barrier permeability and expression of matrix metalloproteinases and tight junction proteins in mice. Particle and fibre toxicology 10:62.
Ottens AK, Stafflinger JE, Griffin HE, Kunz RD, Cifu DX, Niemeier JP. 2014. Post-acute brain injury urinary signature: A new resource for molecular diagnostics. J Neurotrauma 31:782-788.
Paffett ML, Zychowski KE, Sheppard L, Robertson S, Weaver JM, Lucas SN, et al. 2015. Ozone inhalation impairs coronary artery dilation via intracellular oxidative stress: Evidence for serum-borne factors as drivers of systemic toxicity. Toxicol Sci.
Palmer KT, McNeill Love RM, Poole JR, Coggon D, Frew AJ, Linaker CH, et al. 2006. Inflammatory responses to the occupational inhalation of metal fume. Eur Respir J 27:366-373.
Peer D, Karp JM, Hong S, Farokhzad OC, Margalit R, Langer R. 2007. Nanocarriers as an emerging platform for cancer therapy. Nat Nanotechnol 2:751-760.
Porter DW, Hubbs AF, Mercer RR, Wu N, Wolfarth MG, Sriram K, et al. 2010. Mouse pulmonary dose- and time course-responses induced by exposure to multi-walled carbon nanotubes. Toxicology 269:136-147.
Pozzi A, Moberg PE, Miles LA, Wagner S, Soloway P, Gardner HA. 2000. Elevated matrix metalloprotease and angiostatin levels in integrin alpha 1 knockout mice cause reduced tumor vascularization. Proc Natl Acad Sci U S A 97:2202-2207.
Rao X, Zhong J, Maiseyeu A, Gopalakrishnan B, Villamena FA, Chen LC, et al. 2014. Cd36-dependent 7-ketocholesterol accumulation in macrophages mediates progression of atherosclerosis in response to chronic air pollution exposure. Circ Res 115:770-780.

Ren J, Shen S, Wang D, Xi Z, Guo L, Pang Z, et al. 2012. The targeted delivery of anticancer drugs to brain glioma by pegylated oxidized multi-walled carbon nanotubes modified with angiopep-2. Biomaterials 33:3324-3333.
Rivas-Arancibia S, Guevara-Guzman R, Lopez-Vidal Y, Rodriguez-Martinez E, Zanardo-Gomes M, Angoa-Perez M, et al. 2010. Oxidative stress caused by ozone exposure induces loss of brain repair in the hippocampus of adult rats. Toxicol Sci 113:187-197.
Robertson S, Colombo ES, Lucas SN, Hall PR, Febbraio M, Paffett ML, et al. 2013. Cd36 mediates endothelial dysfunction downstream of circulating factors induced by o3 exposure. Toxicol Sci 134:304-311.
Satoh S, Ikegaki I, Suzuki Y, Asano T, Shibuya M, Hidaka H. 1996. Neuroprotective properties of a protein kinase inhibitor against ischaemia-induced neuronal damage in rats and gerbils. Br J Pharmacol 118:1592-1596.
Sawada H, Saito Y, Noguchi N. 2012. Enhanced cd36 expression changes the role of nrf2 activation from anti-atherogenic to pro-atherogenic in apoe-deficient mice. Atherosclerosis 225:83-90.
Shaul PW. 2003. Endothelial nitric oxide synthase, caveolae and the development of atherosclerosis. J Physiol 547:21-33.
Singh R, Mehra NK, Jain V, Jain NK. 2013. Gemcitabine-loaded smart carbon nanotubes for effective targeting to cancer cells. J Drug Target 21:581-592.
Su WY, Jaskot RH, Dreher KL. 2000. Particulate matter induction of pulmonary gelatinase a, gelatinase b, and tissue inhibitor of metalloproteinase expression. Inhal Toxicol 12 Suppl 2:105-119.
Sun Q, Wang A, Jin X, Natanzon A, Duquaine D, Brook RD, et al. 2005. Long-term air pollution exposure and acceleration of atherosclerosis and vascular inflammation in an animal model. JAMA 294:3003-3010.
Takeda S, Sato N, Morishita R. 2014. Systemic inflammation, blood-brain barrier vulnerability and cognitive/non-cognitive symptoms in alzheimer disease: Relevance to pathogenesis and therapy. Front Aging Neurosci 6:171.
Tsai HC, Lin JY, Maryani F, Huang CC, Imae T. 2013. Drug-loading capacity and nuclear targeting of multiwalled carbon nanotubes grafted with anionic amphiphilic copolymers. Int J Nanomedicine 8:4427-4440.
Ueno M, Nakagawa T, Nagai Y, Nishi N, Kusaka T, Kanenishi K, et al. 2011. The expression of cd36 in vessels with blood-brain barrier impairment in a stroke-prone hypertensive model. Neuropathol Appl Neurobiol 37:727-737.
Uittenbogaard A, Shaul PW, Yuhanna IS, Blair A, Smart EJ. 2000. High density lipoprotein prevents oxidized low density lipoprotein-induced inhibition of endothelial nitric-oxide synthase localization and activation in caveolae. J Biol Chem 275:11278-11283.
Ujiie M, Dickstein DL, Carlow DA, Jefferies WA. 2003. Blood-brain barrier permeability precedes senile plaque formation in an alzheimer disease model. Microcirculation 10:463-470.
Van Eeden S, Leipsic J, Paul Man SF, Sin DD. 2012. The relationship between lung inflammation and cardiovascular disease. Am J Respir Crit Care Med 186:11-16.
Vittorio O, Raffa V, Cuschieri A. 2009. Influence of purity and surface oxidation on cytotoxicity of multiwalled carbon nanotubes with human neuroblastoma cells. Nanomedicine 5:424-431.
Walters CE, Pryce G, Hankey DJ, Sebti SM, Hamilton AD, Baker D, et al. 2002. Inhibition of rho gtpases with protein prenyltransferase inhibitors prevents leukocyte recruitment to the central nervous system and attenuates clinical signs of disease in an animal model of multiple sclerosis. J Immunol 168:4087-4094.
Wang W, Deng M, Liu X, Ai W, Tang Q, Hu J. 2011. Tlr4 activation induces nontolerant inflammatory response in endothelial cells. Inflammation 34:509-518.
Wong WT, Ng CH, Tsang SY, Huang Y, Chen ZY. 2011. Relative contribution of individual oxidized components in ox-ldl to inhibition on endothelium-dependent relaxation in rat aorta. Nutrition, metabolism, and cardiovascular diseases : NMCD 21:157-164.

Wraith KS, Magwenzi S, Aburima A, Wen Y, Leake D, Naseem KM. 2013. Oxidized low-density lipoproteins induce rapid platelet activation and shape change through tyrosine kinase and rho kinase-signaling pathways. Blood 122:580-589.
Wu CH, Cao C, Kim JH, Hsu CH, Wanebo HJ, Bowen WD, et al. 2012. Trojan-horse nanotube on-command intracellular drug delivery. Nano Lett 12:5475-5480.